Optimizing Electricity Generation Portfolios with Intermittency: Does Delayed Externality Pricing Cause Lock-In Regret?

Thomas Lee

Advisors:
Professor Monique Guignard-Spielberg
Dr. Andrew E. Huemmler

December 10, 2017
Philadelphia, Pennsylvania

SENIOR CAPSTONE THESIS

Department of Computer and Information Science
School of Engineering and Applied Science

UNIVERSITY OF PENNSYLVANIA

Abstract

To what extent does delaying carbon pricing, via a carbon tax or emissions trading, lead to locked-in investments of fossil fuel power generation assets that prevent later adoption of renewable energy? The literature review integrates insights from distinct domain areas of climate science, economics, and power systems, while connecting underlying methodological tools to roots in computer science. This thesis then develops original research, in order to analyze the mathematical conditions and properties of economic path dependence in an electric generation portfolio that includes both intermittent load and renewable resources. The analytical results suggest that the possibility and magnitude of carbon lock-in under more rigorous conditions (i.e. carbon price additionality, load intermittency, and renewables intermittency) are less than what is implied by prior literature. The original research also quantifies the extent of carbon lock-in specifically in the power grid of the PJM Interconnection, with a particular focus on natural gas combined-cycle buildout, through a constrained linear programming (LP) capacity expansion optimization model using hourly-resolution time series data of load and generation with onshore wind and solar photovoltaics. Energy storage modeling is included as a limiting case, for robustness checking. The main numerical result is that the presence of existing dispatchable power capacity, especially nuclear power, vastly diminishes the carbon lock-in effect's extent down to a negligible magnitude.

Acknowledgements

I would like to thank my thesis advisors Professor Guignard-Spielberg and Dr. Huemmler. Thanks to Adam Keech of PJM for industry insight and feedback on modeling results, to Dr. David Bielen and Kelly Eurek of NREL for helpful discussion about optimization modeling and multi-period assumptions in the ReEDS model, and to Dr. Lance Noel for comparative feedback on my initial numerical results. Thanks to Professor Steven Kimbrough for helpful feedback to a presentation of my results. I also want to thank Christina Simeone of the Kleinman Center for Energy Policy as well as Jake Noonan for helpful feedback on earlier drafts of the thesis. Any remaining errors or omissions here are mine alone.

Table of Contents

1. Introduction

Electric power grids are facing substantial transformation, both globally and in the PJM Interconnection – which is the largest competitive wholesale electricity market in the United States, covering D.C. and 13 states including Pennsylvania, New Jersey, and Maryland. The innovation of horizontal drilling and hydraulic fracturing or "fracking" have spurred a North American natural gas production boom, stabilizing natural gas commodity prices to historically low levels [1]. Combined with efficiency improvements for combined-cycle power plants, the low natural gas price environment is driving significant buildout and planned future additions of new gas-fired power generation capacity in the PJM region: about 15 gigawatts (GW) of new gas-fired combined-cycle capacity is expected to come online within 2017-2018, along with an additional 22 GW under development [2].

While natural gas is often seen as a "bridge fuel" due to creating significantly lower carbon dioxide emissions than coal, the methane that may be leaked as fugitive emissions during the natural gas supply chain has a much higher global warming potential than carbon dioxide [3]. Meanwhile, optimization modeling by Noel et al. [4] suggests that the least-cost PJM grid system incorporating climate and health externalities would include higher levels of renewables than currently planned. For this reason, the trend of rapid natural gas development may raise concerns about path dependency for the deployment of renewable energy.

Path dependency might occur because once investment capital costs are incurred, these sunk costs do not matter for future decisions. Erickson et al. [5] provide a framework to assess how high a carbon price needs to be in order to escape carbon lock-in, implying that carbon prices lower than such a level would likely lead to carbon lock-in. Such a perspective is consistent with Unruh's [6] theoretical framework of institutional inertia. However, optimization modeling by Mignonge et al. [7] suggests that the natural gas combined-cycle power capacity built out under a medium carbon price regulatory environment may still be optimal under a substantially more stringent policy scenario with an increasing carbon price. In turn, this result might imply that any amount of carbon lock-in due to natural gas combined-cycle generation assets could be limited.

In this context, this thesis seeks to contribute to the understanding of carbon lock-in by reconciling the conceptual gap among [5][6] and [7]. Moreover, while these prior studies all take a global or national level perspective, this thesis seeks to contribute regional relevance by focusing on PJM, a region notable both for its geographical coincidence with the Marcellus Shale formation and for the sophistication of its wholesale electricity markets. As well, to answer this question about lock-in, this thesis must also explore the fundamental question: What is the optimal set of investments in electricity generation technologies, given these resource types have very different cost structures, intermittency profiles, and environmental impacts?

2. Literature Review

In order to rigorously assess the possibility of carbon lock-in, this thesis begins with an in-depth literature review of the relevant domain systems: global climate change and power systems. The survey serves to establish the reasonableness of the major methodology choices made by the thesis, i.e. modeling climate externalities as a carbon price, and justifying model simplifications of power systems' physical and economic complexities. Finally, the survey examines concepts relevant to economic path dependence, drawing on analogies and connections to concepts from mathematics, physics, and economics, as well as the regret function often used in computer science.

The literature review also reveals how the quantitative study of both domain systems are fundamentally enabled by computational science – for example, the first civilian application of the University of Pennsylvania's ENIAC was numerical weather prediction, and several artificial intelligence algorithms have been applied to power system optimization.

2.1 Climate Externalities

The history of meteorology and climate science is linked with the history of computer science. The Electronic Numerical Integrator and Computer (ENIAC) was developed at the University of Pennsylvania's engineering school and was the first multi-purpose electronic digital computer, completed in 1945. Weather forecasting was the very first non-military usage of this ENIAC, under a research program first initiated in 1946 [8]. John von Neumann, a core contributor to the Manhattan Project and leader of this early research effort, "selected weather forecasting over many other possible applications for the earliest electronic digital computers because it bore a strong mathematical similarity to nonlinear fluid dynamics problems that cropped up in nuclear weapons design" [9].

Research in numerical weather prediction led to the development of general circulation models (GCM) enabling the study of long term climate patterns, which von Neumann called "the infinite forecast" [9]. General circulation models at their core solve a system of differential equations known as the primitive equations, which describe fluid motion in the atmosphere or ocean [10]. Algorithmically, these differential equations can be solved using numerical techniques like the finite-difference methods [8]. The primitive equations in atmospheric science and oceanography must include a continuity equation to describe conservation of mass, the first law of thermodynamics that captures conservation of energy, three momentum equations to capture conservation of momentum along each coordinate axis, and an equation of state such as the ideal gas law $PV = nRT$ [11]. The continuity equation states that mass is conserved during fluid transport; where ρ is density and u is the velocity vector [10]:

$$\frac{\partial \rho}{\partial t} + \nabla \cdot (\rho u) = 0$$

The first law of thermodynamics ensures conservation of energy through external drivers of the heat flux dQ/dt that represents "the solar heating, the albedo of the earth, and the molecular heating" [11]. The absorbed energy from solar radiation is some function of the incoming energy and the surface albedo, e.g. $(1 - \alpha)S$; this is balanced with the re-emitted

energy, e.g. for an ideal gray body the emitted energy is proportional to its emissivity ε and the fourth power of temperature according to the Stefan-Boltzmann law $E = \varepsilon\sigma T^4$ [12]. Realistic climate models include detailed modeling of these sources of thermodynamic flux as well as feedback mechanisms; for example, an increased atmospheric temperature reduces the area of snow cover and ice pack, which reduces surface albedo, thereby further increasing temperature [13]. The thermodynamic equation for the case of a compressible fluid like the atmosphere can be written as the following, where c_p is the specific heat capacity [11],:

$$c_p \frac{dT}{dt} - \frac{RT}{p}\frac{dp}{dt} = \frac{dQ}{dt}$$

Applying scale analysis to momentum balance yields the geostrophic balance equation, which arises from balancing the inertial Coriolis force due to angular planetary rotation with the pressure gradient force [10]. In the Coriolis parameter $f = 2\Omega \sin\varphi$, where Ω is the upwards-direction rotation vector and φ is the latitude angle, $\Omega \sin\varphi$ is the "vertical component of the Earth's rotation rate"; the vertical component is the "only component that matters" due to the "thinness" or aspect ratio of the Earth's atmosphere and ocean compared to the planet's diameter [10]. The geostrophic balance equation states, where $\hat{z}$ is the upwards unit vector:

$$fu = \frac{1}{\rho}\hat{z}\times\nabla p$$

By applying a large-scale approximation with negligible vertical acceleration (i.e. ignoring "vigorous small-scale systems" like tornados and thunderstorms), the hydrostatic balance equates the vertical pressure gradient with the gravitational force [10]:

$$\frac{\partial p}{\partial z} = -g\rho$$

Combining the horizontal geostrophic balance with the vertical hydrostatic balance leads to the thermal wind balance, which relates wind pressure gradients to the horizontal temperature gradients [14]. Using log-pressure coordinates, where u, v are the horizontal velocities, the thermal wind balance equation states [14]:

$$\frac{\partial u_g}{\partial \ln p} = \frac{R}{f}\frac{\partial T}{\partial y}, \qquad \frac{\partial v_g}{\partial \ln p} = -\frac{R}{f}\frac{\partial T}{\partial x}$$

Modern atmosphere-ocean general models, such as those considered by the Intergovernmental Panel on Climate Change's (IPCC) Assessment Reports, typically utilize a three-dimensional grid to model the dynamics in integrated atmosphere, ocean, land, and sea ice subsystem, as well as their response to "greenhouse gas (GHG) and aerosol forcing" at seasonal, decadal, or longer-term timescales [15]. By the Fifth Assessment Report of 2013, the type of state-of-the-art models are more detailed, termed earth system models, which also incorporate submodules for the effects and "interactive" feedback of aerosols, various mechanisms of ocean-atmosphere-land coupling, and biogeochemical cycles, including the carbon, sulfur, and ozone cycles [15].

By building on general circulation and earth system models, integrated assessment models (IAM) also incorporate socioeconomic modeling and can be used to quantify the marginal damage from greenhouse gas emissions, i.e. the social cost of carbon (SCC). A baseline

trajectory of emissions $(E_0, \dots, E_t)$ physically results in a trajectory of temperature changes ΔT_t, which when integrated over time and properly discounted leads to the total "discounted present value of damages" [16]:

$$PVD = \int_0^\infty D(\Delta T_t)dt$$

Then the derivative with respect to the amount of emissions E_0 measures the sensitivity of the present value of damages to an increase in emissions level. This derivative represents the marginal damage from each extra unit of emissions, and is the social cost of carbon [16]:

$$MDCC = \frac{\partial PVD}{\partial E_0}$$

In practice, estimation of the damage functions is an area of active study and source of uncertainty, and is in large part an empirical question. Damages from climate change encompass "losses of gross domestic product (GDP)" as well as "dollar-equivalent costs of possible climate-related increases in morbidity, mortality, and social disruption" [17]. For example, Hsiang in [18] and [19] formalizes the quantification of climate effects on social and economic outcomes in terms of econometric theory and methodology. [29] provides an extensive survey of various econometric models to estimate climate change damage functions for 140 countries and regions.

In addition, the choice of the social discount rate is extensively studied in literature and faces substantial controversy. A low discount rate means utility for a future generation is valued highly, which would lead to a high social cost of carbon. Goulder and Williams [21] distinguish between a "social-welfare-equivalent" discount rate to determine whether a policy improves social welfare, versus a "finance equivalent" discount rate to determine whether a policy leads to a Pareto improvement; this distinction, the authors argue, separates out the prescriptive (where the the rate may be based on intergenerational ethical considerations) versus descriptive (where the rate may reflect market interest rates or returns) role of the discount rate.

Amidst modeling uncertainty, a survey of different social cost of carbon studies by Gollier and Pachon [22] suggest that a carbon price of around \$40 / ton CO_2 is reasonable for the present day. This estimate is consistent with a consumption-based capital asset pricing model (CCAPM) of asset pricing theory from financial economics, by considering the counteracting effects of a positive correlation beta between climate damages and consumption [23]. A positive "climate beta" implies a high discount rate but also larger climate damages in states of high growth; numerical analysis suggests the net effect of consumption-damage correlation is to raise the price of carbon [22]. This magnitude is also consistent with the social cost of carbon estimates conducted by the Obama administration's Interagency Working Group [24], which at a 3% discount rate estimates a \$42 / ton CO_2 social cost for the year 2020 and a \$50 / ton CO_2 cost for 2030, while also recognizing the tail risks of low-probability high-impact climate events with a 95th percentile social cost estimate of \$123 / ton CO_2 and \$152 / ton CO_2 for 2020 and 2030, respectively.

A more recent obstacle in estimating and interpreting the social cost of carbon is the regional scope of damage functions, since global climate change involves significant externalities that cross national borders. Gayer and Viscusi [25] advocate that regulations should

focus just on domestic-only impacts, by arguing "the benefits of reducing U.S. GHGs across national borders are accompanies by no intergovernmental grants from other countries to the United States"; instead, the authors argue that a more accurate social cost of carbon must be based on "actual empirical support rather than optimistic assumptions of full global reciprocity." This viewpoint is reflected in active policy discussions; for example, the 2017 proposal for repealing the Environmental Protection Agency's (EPA) Clean Power Plan relies on an impact analysis which "shifts the focus to the domestic (rather than global) social cost of carbon," by only considering "direct impacts of climate change that are anticipated to occur within U.S. borders" [26].

However, a response article [28] in the same journal explains that the game theoretical reciprocity so desired by Gayer and Viscusi has actually been empirically achieved through extant international diplomacy as the "Obama administration has strategically incorporated the global SCC into climate negotiations, most recently harmonizing its global SCC valuation with Canada and Mexico." Howard and Schwartz [29] point out that various official international climate frameworks and unofficial legal norm-setting pathways do fulfill Gayer and Viscusi's speculative reciprocity criterion. Furthermore, the "decreasing marginal utility of consumption and heterogeneity in regional wealth" means the mainstream SCC estimates already favor higher-income nations [29].

2.2 Power System Optimization

The National Academy of Engineering [30] hailed "electrification" as the top greatest engineering achievement of the 20th century, raising the standard of living for many populations and enabling the innovation of numerous technologies, including digital electronic computers. Modern electric power systems broadly consist of the generation, transmission, and distribution sectors, and most parts of the bulk power system utilize the three-phase alternating current (AC) system [31]. While electric power enabled the development of computers, in turn computing technology also enabled the use of software automation, control, and optimization for power systems, including via supervisory control and data acquisition (SCADA) systems [32] and optimization algorithms for various planning and operational problems [33].

Electric power optimization models can be broadly divided into different model types dealing with electric system planning or operation at different timescales: capacity expansion, grid operation (e.g. unit commitment and economic dispatch), and network reliability models [34]. According to Boyd's [34] high-level classification:

- Capacity expansion models (such the Energy Information Administration's NEMS or the National Renewable Energy Laboratory's ReEDS) "simulate generation and transmission capacity investment" under different scenarios of policy and technology trajectories.
- Operational models for unit commitment or economic dispatch (such as commercial software PROMOD and PLEXOS) focus on finding the least cost dispatch of a network of existing generators and transmission.
- Network reliability models focus on steady-state power flow or transient dynamics to assess the operational reliability of the transmission system, including responses to contingency fault events.

In general terms, the physical detail and temporal resolution is usually inversely related with the model time horizon: capacity expansion modeling usually considers power system changes over the course of years to decades and so rely on coarser time resolutions from time-of-day to seasons, while commitment and dispatch models have shorter horizons but model the grid system usually at five-minute to hourly time steps (Boyd). For example, the Electricity Market Module (EMM), a component of the National Energy Modeling System (NEMS), abstracts away from engineering aspects such as power flow or reactive power [35].

Frew and Jacobson [36] directly address the methodological tradeoffs between modeling complexity in "temporal resolution and extent, spatial resolution and extent, and model complexity." For example, most of the capacity expansion models surveyed incorporate "inter-regional" but not "intra-regional" transmission constraints, in the form of edge weights in a simplified graph network. In addition, some but not all capacity expansion models utilize representative "time slices" to reduce problem dimensionality, but leads to challenges in accurately modeling specifically state-dependent aspects like energy storage.

In practice power system models used by grid system operators often incorporate both considerations of alternating current physics, i.e. AC power flow, as well as production cost economics [37]. In particular, "[p]ower flow study is the most frequently carried out study performed by power utilities" at "almost all the stages of power system planning, optimization,

operation, and control" [38]. Therefore, it may be useful to highlight some aspects of power flow analysis, in order to understand the nature of any simplifying assumptions that abstract away from these details.

The physics of electric circuits are fundamentally governed by Kirchhoff's voltage law (sum of voltages around any closed network is zero) and Kirchhoff's current law (sum of currents meeting at any node is zero), which can be derived as special cases of Maxwell's equations of electromagnetism [39]. In an AC circuit, current and voltage values have sinusoidal oscillations at the same frequency, which is 60 Hz in North American bulk power systems. The voltage and current waveforms can each be identified as functions of amplitude and phase angle – in both trigonometric and phasor forms [40]:

$$v(t) = V_m \cos(\omega t + \phi_v) \Leftrightarrow V_{rms} = \frac{V_m}{\sqrt{2}} e^{j\phi_v}, \qquad i(t) = I_m \cos(\omega t + \phi_i) \Leftrightarrow I_{rms} = \frac{I_m}{\sqrt{2}} e^{j\phi_i}$$

The analog of the direct current case of power $p = iv$, the complex power in an AC circuit is given by $S = V_{rms} I_{rms}^* = P + jQ$, where I^* denotes the complex conjugate of the phasor and P and Q are called the real (or active) and reactive power components, respectively [40]. Steady state operation of the power system requires the active and reactive power components to be balanced at each node in the network; this instantaneous balance corresponds to conservation of energy, incorporating potential energy stored in inductive elements' magnetic fields as well as capacitive elements' electric fields. The general form of the power flow equations state, in the notation of Momoh [41]:

$$S_i^* = P_i - jQ_i = V_i^* \sum_{k=1}^{n} Y_{ik} V_k$$

Where each element Y_{ik} is the admittance (reciprocal of the complex impedance, measured in ohms) between nodes i and k, and depends on the topology of the transmission system and the inductances and capacitances of its components. By analogy, Ohm's law in DC gives $v = ir$ or $i = v/r$, and so each $Y_{ik} V_k$ term can be thought of as representing an electrical current value.

The nature of the admittance matrix Y depends on the part of the transmission grid and the problem context. For passive elements like transmission lines, or for problem contexts that consider the power system for a fixed grid configuration, the elements of the admittance matrix (which can be described in terms of separate real conductance and imaginary susceptance matrices) are constant values [37]. On the other hand, various active transmission elements, including "phase shifting transformers, switched capacitors/reactors, or power electronic flexible AC transmission system (FACTS) devices," will have variable and controllable admittance values [37]. In fact, the "nonlinear behavior of electronic-based devices such as FACTS" introduces nonconvex or other mathematically complicating aspects to power flow [42].

AC power flow involves a large-scale nonlinear system of equations – in practice a power grid can have on the order of thousands or more nodes. Thus solution methods for power flow equations usually utilize numerical iterative algorithms. In the beginning of digital computers, the Gauss-Seidel algorithm was used for solving power flows, but convergence becomes much slower at large system sizes; in comparison, the Newton-Raphson algorithm approach has

superior time complexity and is most commonly used today [37]. The general Newton-Raphson algorithm finds roots of function by iteratively updating the error step and solution vectors [41]:

$$f\left(\boldsymbol{x}^{(v)}\right) + \boldsymbol{J}^{(v)}\Delta\boldsymbol{x}^{(v)} \approx 0 \Longrightarrow \Delta\boldsymbol{x}^{(v)} \approx -\left[\boldsymbol{J}^{(v)}\right]^{-1} f\left(\boldsymbol{x}^{(v)}\right)$$
$$\boldsymbol{x}^{(v+1)} = \boldsymbol{x}^{(v)} + \Delta\boldsymbol{x}^{(v)}$$

Where J is the Jacobian matrix with elements $\boldsymbol{J}_{i,j} = \partial f_i / \partial f_j$. Numerically, the matrix inversion step suggests the Jacobian may an important factor in the calculation speed for each iteration step. In fact, the fast-decoupled power flow method improves solution efficiency by exploiting a matrix sparsity structure, by assuming that changes in real power ΔP are relatively insensitive to changes in voltage magnitude $\Delta|V|$ and that changes in reactive power ΔQ are relatively insensitive to changes in phase angle $\Delta\delta$ [41]. This method assumes the off-diagonal N and M matrix blocks are 0 to decouple the system into two equations with lower dimensionalities, compared to the original full Jacobian matrix [41]:

$$\begin{bmatrix}\Delta P \\ \Delta Q\end{bmatrix} = \begin{bmatrix}H & N \\ M & L\end{bmatrix}\begin{bmatrix}\Delta\delta \\ \dfrac{\Delta|V|}{V}\end{bmatrix}$$

Further simplification can be achieved when assuming that a transmission component's resistance (real component) is relatively small compared to its reactance (imaginary component), resulting in a linearized, "direct current" or "DC" power flow model [41]. To be sure, such a direct current or DCOPF formulation, which effectively assumes "all voltage magnitudes are fixed and all voltage angles are close to zero," does not refer to a power grid physically running on DC, but rather a linearization approximation for a full AC network [37].

Newer solution methods to the power flow equations beyond the Newton-Raphson method have paralleled developments in computer science. Utilizing the ability of artificial neural networks to model complex nonlinear functional forms, Paucar and Rider [43] demonstrate a method of using multilayer perceptron neural networks using inputs of the nodal voltage magnitudes and angles in the power flow problem, showing superior on-line solution speed over Newton-Raphson. Rather than using a multilayer feedforward neural network architecture, which may have a slower training process, Krishna and Srivastava [38] use counterpropagation neural networks to solve the full AC power flow problem to compute nodal voltage magnitudes and angles. Conceptually, these artificial intelligence methods may preserve greater physics details by training neural networks to accommodate more complicated functional mappings, compared to other approaches that rely on domain-specific simplifications such as the Jacobian matrix decoupling or DC linearization.

Building on the physics of AC power flow, the class of problems known as optimal power flow seeks to find "the optimal solution to an objective function subject to the power flow constraints and other operational constraints" [37]. In this sense, solving power flow equations constitutes a part of optimal flow optimization problems, which in turn can have various objective functions depending on the specific context, including: fuel cost minimization, active power loss minimization, reactive power loss minimization, or maximum power transfer [41].

Cain et al. explain that the alternating current optimal power flow problem (ACOPF) possesses economical, electrical, and computational complexities; these complexities arise

because efficient market equilibrium necessitates "multi-part nonlinear pricing," the nature of alternating current introduces nonlinearities in terms of transcendental functions, and the computational optimization problem includes both continuous and binary variables, e.g. start up and shut down decisions for generators. In short, the optimal power flow problem is a "large-scale highly constrained nonlinear nonconvex optimization problem" [42]. Adding to the complexity are security-constrained optimal power flow and unit commitment problems, to ensure reliability under contingency events to satisfy the N – 1 reliability criterion (where the system must withstand any single credible contingency), which can be seen as instances of robust optimization [44].

Many optimization algorithms have been applied to solve optimal power flow, including nonlinear programming, quadratic programming, linear programming, Newton-based algorithms, and interior point methods [41][42][44]. However, many of these more conventional optimization methods used for optimal power flow share a common "gradient-based" optimization approach by "linearizing the objective function and the system constraints around an operating point" [42]. These limitations have inspired optimization solution methods based in artificial intelligence. An approach inspired by evolutionary algorithms, i.e. particle swarm optimization (PSO), is demonstrated to solve optimal power flow problems in a "derivative-free" way [42]. Similarly, [45] applies another evolutionary algorithm, i.e. a genetic algorithm (GA) approach, to solve optimal power flow with both continuous and discrete control variables. As well, [46] applies neural networks to solve optimal power flow, demonstrating results of fast computation times by exploiting massively parallel computing structure.

2.3 Optimality Versus Markets

It is important to recognize what "is" is a distinct issue from what "ought" to be. The usage of optimization modeling for the electric power grid long-term planning problem raises the conceptual question of whether the optimization results should be treated as prescriptive recommendations of what ought to be done under various assumed scenarios, or predictions of real-world outcomes that will result from these scenarios. For example, according to the the NEM EMM's documentation, the electricity capacity planning (ECP) submodule "uses a linear programming (LP) formulation to determine planning decisions for the electric power industry," explaining that this approach "simulates least-cost planning and competitive markets by selecting strategies for meeting expected demands and complying with environmental restrictions that minimize the total discounted present value of the investment and operating costs over the planning horizon" [35]. Various other electric capacity planning models also use an optimization approach, sometimes referred to as the social planner's perspective. However, for competitive wholesale market regions like the PJM Interconnection, it is not theoretically guaranteed that realized market outcomes identically correspond to optimization solutions. Therefore, it is useful to consider the nature of electricity markets and their potential structural deviations from optimality.

Garcia et al. [47] explain the historical restructuring of the electric industry as resulting from technology innovations in natural gas combined cycle power plant efficiency, leading to decreased validity in the economies of scale argument that justified regulating the electric generation suppliers as utilities with legal monopoly. In place of vertically integrated utilities covering all generation, transmission, distribution, and retail, the generation of electric power in restructured jurisdictions is now allocated through competitive markets based on locational marginal pricing (LMP) which accounts for the "cost of transferring power from one location to another" under conditions of network congestion [47].

More abstractly, Ethier et al. [48] present a generic cost minimization problem for the grid system operating overseeing an electricity market. The u vector represents real power output from generators, and c_i is each generator's associated cost function related to the power output. The vector x represents node voltages, and the equality constraint set can therefore represent power flow equations (i.e. to satisfy Kirchhoff's laws such that net power injected equals net power leaving each node). The inequality constraints can encompass limits including node voltages, real and reactive power, and transmission capacity:

$$\min_{u} f(u) = \sum_i c_i(u_i) \text{ s.t. } g(x,u) = 0, \quad h(x,u) \leq 0$$

This formulation in an electricity market setting becomes identical to the "social planner's welfare maximization problem" if the cost functions c_i are true marginal costs for each generator and load demand at each node is fully inelastic [48]. In the setting of a regulated utility structure, each generator's true marginal cost can be perfectly known as a function of its power output. In comparison, in a competitive electricity market, the cost functions c_i from the system perspective are those that are revealed by the generation firms' submitted offer curves. Consequently, the "cost-revealing properties of the chosen market institution are fundamental to achieving an optimal dispatch" in a competitive market setting [48].

Meanwhile, the "high levels of industry concentration make the occurrence of strategic behavior almost inevitable," leading economic analyses of electricity markets to often utilize game theory to model Bertrand (price-based) or Cournot (quantity-based) competition [47]. The tractability of these models to account for strategic bidding behavior may require tradeoffs to simplify some "non-trivial features such as loop-flow and reactive power" [47].

In this context, if an electricity market can be designed to perfectly minimize the strategic exercise of market power, i.e. for the marginal prices to be truthfully revealed, then the actual market outcome would approach the socially optimal solution assuming an omniscient, benevolent social planner. More generally from microeconomic theory, the first welfare theorem (stating that under certain conditions including costless information, a competitive equilibrium is Pareto optimal) and second welfare theorem (stating that any Pareto optimal allocation can be achieved by adjusting a competitive equilibrium with lump-sum redistributions) "establish a connection between the competitive equilibrium and the social planning problem" [49]. Specifically, after solving an optimization problem from the social planner's perspective, the welfare theorems can be used to interpret the resulting resource allocation "quantities as those arising from a competitive economy" [49]. In other words, it may be possible to interpret electricity optimization as not only normative or prescriptive (i.e. what ought to be done) but also in a sense predictive (i.e. what will be done in a perfectly competitive market responding to economic price signals).

Figure 1: Map of the PJM geographical footprint as of 2017. Source: PJM.

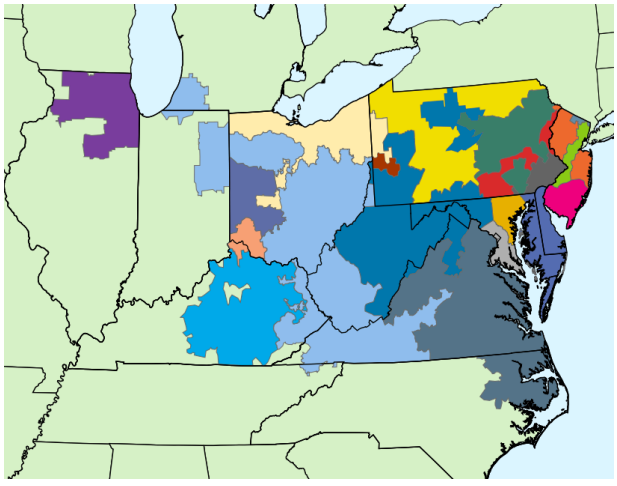

2.4 Renewable Energy Intermittency

Further complexities in the power system arise with the introduction of variable renewable energy sources, which exhibit intermittency. Hart et al. [50] define intermittency as comprising of "both variability and uncertainty" components. Statistically, variability is the heterogeneity between different members in a statistical population (which in the case of energy resources occurs along the time dimension), and thus "is usually not reducible through further measurement or study" [51]. In contrast, uncertainty arises from "lack of perfect information" about the "true value" of a parameter for a particular member of the population [51]. In operational practice, the difference between variability and uncertainty in the power system context is that a variable but predictable energy resource would be managed with "careful day-ahead scheduling" that incorporates the forecast predictions, compared to an uncertain resource that would also require "the need for additional reserves [52].

As a direct consequence of physics and statistics, intermittency is reduced via aggregation or diversification of different renewable energy geographic locations, i.e. achieving "statistical smoothing of a single technology employed over large geographical areas," as well as different technology types, i.e. which "utilize different (and often uncorrelated) renewable resources" [50]. This diversification effect occurs with sufficiently small correlations, e.g. for a simple average of two random variables the total variance is:

$$Var[0.5(X+Y)] = (0.5)^2[\sigma_X^2 + \sigma_Y^2 + 2Cov(X,Y)]$$

For a single resource type, X, Y can be scalars representing the realizations of energy output within the same time period at different locations, so a decrease in portfolio variance can represent a decrease in intra-period uncertainty. In comparison, X, Y also can each represent a perfectly deterministic vector of energy production across time, i.e. with no uncertainty to start with, so that portfolio diversification represents a decrease in inter-period variability.

Physically, the relative lack of perfect correlations between wind power units at "short distances and short time scales" (on the order of one minute temporally and within one wind farm spatially) arises due to the averaging of "turbulence and terrain effects," while low or negative correlations for wind power at much greater time and spatial scales occur because large scale weather systems like atmospheric pressure systems occur on scales roughly on the order of 1,500 km [50]. In contrast, the variability of solar power is driven by a combination of deterministic cycles in the clear-sky solar irradiance, which is ultimately driven by the physics of planetary motion, as well as stochastic fluctuations caused by random cloud cover [50].

Based on this insight about intermittency's two distinct aspects, Hart et al. develop a taxonomy to categorize three classes of model fidelity when studying intermittent energy sources. Zeroth order models only account for average resource availability, so the data types used are likely to be "[a]nnual or seasonal means" indexed just by resource type and location. First order models incorporate the time variability of resource availability, and thus require more detailed time series data that also possess a time dimension. Finally, second order models additionally incorporate the information set available at each point in time of relevant operational decisions, and so require both time series data of the energy resource as well as the available forecasts and associated uncertainties at each point in time.

In addition to hardware technologies like energy storage, the software of grid operators' institutional procedures and control algorithms can help integrate variable renewables into the grid more efficiently; such system operations improvements can be thought of as addressing the uncertainty component of intermittency. In particular, "[i]ntegrating advanced forecasting techniques into fast market operations, the control room, and other standard operating practices can help predict the amount of [renewable energy] available to the system" [52]. For example, various algorithmic methods have been applied to the problem of renewable energy forecasting. Orwig et al. [53] provide a detailed overview of the current state of renewable energy (wind and solar) forecasting and its application to power systems operation, surveying numerical weather prediction (NWP) techniques to predict meteorological variables and statistical methods (including AI algorithms and Kalman filtering) which incorporate these weather variables to predict actual electricity output.

Although solar power forecasting is challenging due to the difficulty in predicting short-term cloud shadowing, researchers are developing new machine learning approaches [53]. For example, Sharma et al. [54] apply principal component analysis (PCA) for dimensionality reduction to a suite of weather variable forecasts from the National Weather Service, including temperature, dew point, wind speed, sky cover, precipitation, and humidity; then linear regression and SVM (support vector machine) using various kernel functions are applied to these weather variables to predict solar intensity. Chakraborty et al. [55] provide another ensemble algorithm to predict photovoltaic power generation via Bayesian model averaging on three individual predictors, based on naive Bayes, k-nearest neighbors, and a motif-based discretization classifier.

Abstracting away from some of these exact implementation details, the modeling literature that covers the longer time horizon for capacity expansion often incorporate Hart's "second order" uncertainty effects as requirements for backup reserves that may increase as a function of the level of variable renewables. For example, the aforementioned (ReEDS) optimization model incorporates constraints for both reserve margin, i.e. the percentage amount of "firm capacity in excess of the expected peak load" which is usually 15% in the U.S, as well as operating reserve requirements [56]. According to NREL, various categories of operating reserves are designed for different aspects of reliability but are all required for the reliable operation of the grid in the face of load and generation uncertainties. Contingency reserves provide backup for any "unanticipated change to the operational status of generators or transmission lines due to unforeseen outages," and in practice can represent a combination of "spinning reserves" (which are generators spinning at grid frequency ready to provide power output), "interruptible load", or "quick-start units" [56]. Capacity expansion models can model this constraint as a percentage of load demand. Frequency regulation reserves ensure that real-time mismatches between generation and demand are balanced, and can also be modeled as a percentage of load demand [56]. "Variable [renewable energy] forecast error reserves" ensure system reliability through any forecast errors of wind and solar PV output; the approach taken by the ReEDS model is to increase this forecast error reserve requirement as the deployment share of wind and solar increase [56]

What the literature of renewables-incorporating electric grid models have revealed is a gap between alternate visions of the future power grid. On the one hand, studies like Jacobson et

al. [57] demonstrate the technical and economic feasibility of supplying energy systems with 100% of energy (including not just electric power but also heating, cooling, and transportation) sourced from wind, water, and sun while addressing resource intermittency using existing energy storage technologies. Jacobson et al. account for the intermittency nature of renewables by using a meteorological model to predict wind and solar resources worldwide in a time resolution of 30 seconds for every 5 years, and then matching the wind and solar resource time series with hourly-resolution load data. Within this grid integration model, "matching large differences between high electrical demand and low renewable supply" is achieved by various combinations of concentrating solar power (CSP) coupled with energy storage, batteries, or changes in hydropower operating profiles [57].

On the other hand, studies like Hirth [58], looking at the European grid, suggest that an optimized (i.e. least cost, according to a linear program formulation) grid configuration would entail a much lower percentage of variable renewable energy, effectively because higher levels of renewables generation exhibit decreasing returns to scale. Moreover, [59] argues that studies with high renewables penetration scenarios like 100% overestimate the certainty and "large-scale availability" of "energy storage, demand response, and unconstrained transmission" for load balancing, so that the economic effects of renewables intermittency are not fully addressed.

Within the PJM region, Budischak et al. [60] demonstrate the resource adequacy of meeting hourly load during 99.9% of the time by using purely wind, solar, and storage. However, [61] also examines PJM but instead includes conventional generation sources, finding that the least cost solution contains much lower levels of wind and virtually no solar compared to Budischak et al. This result is still consistent with the least-cost optimization findings of the aforementioned [2]. An industry study by PJM itself [62], which does not consider any economic costs, finds that operational limits exist beyond roughly 20% of renewable penetration, with the feasible high-renewables scenario mostly consisting of wind.

An aspect that may be ignored by the least-cost optimization modeling approach is that renewables like wind and solar have very low operating costs, and therefore can provide hedging value to future fluctuations in fuel prices. This intuition is in line with the notion of diversification in modern portfolio theory. Bolinger [63] differentiates between the quantity resource risk of renewable generators with the primarily price-based resource risk of gas-fired generators, in order to quantify "probability of exceedance" projections (using forecasts from historical and options-based implied volatility estimates) of when wind generation becomes less volatile over longer time periods due to statistical averaging just as gas-fired generation continues to face commodity price risk. An NREL study by Jenkin et al. [64] demonstrates using an hourly production cost model that increasing the share of renewable energy sources serve to "significantly reduce the exposure of electricity costs to natural gas price uncertainty," which is particularly important for longer time horizons because "it is difficult and rare to be able to lock in financial or physical supply contracts of 10 years or more for natural gas" in order to replicate the same risk hedging. Further, since "ability to hedge using financial or physical instruments is limited by a lack of knowledge, high transaction costs, or a lack of availability," heterogeneous customers may individually value the hedging value of renewables even more [64].

2.5 Path Dependence and Carbon Lock-In

Path dependence, where the evolution of a system over time significantly depends on its past history, occurs in many contexts. For example, solutions to differential equations depend on their initial conditions, so this path dependence property would generally apply to dynamical systems, perhaps trivially so. In chaos theory, one defining characteristic of a chaotic system is "sensitive dependence on initial conditions": for a metric space X and a relation $T: X \to X$ to constitute a chaotic system, there must exist an $\epsilon > 0$ such that $\forall x \in X$ and $\forall \delta > 0$, $\exists y: d(x, y) < \delta$ as well as $d(T^n x, T^n y) > \epsilon$ for some n [65]. In other words, in such a system "small" differences between system states will continue to be "large" after time.

Many physical systems exhibit path dependence of equilibrium states, often known as hysteresis. Hysteresis can be thought of as "a lagging to respond when the system is prompted to change by a control parameter" [66]. For example, magnetic hysteresis leads a ferromagnetic material to retain magnetization after the external magnetic field is removed, requiring an opposing magnetic field to realign the magnetic domains and thereby trace out a hysteresis loop – a property underlying magnetic data storage [67]. In electrochemical energy storage, nickel-cadmium and nickel-metal-hydride batteries are well known to exhibit a "memory effect", where batteries "lose usable capacity" if they are "only partially discharged" [68].

In economic systems, path-dependence can arise due to increasing returns to adoption, where greater and earlier adoption of a particular technology benefits from a positive feedback loop of either learning-by-doing improvements or network standardization effects, which in turn spur further adoption [69]. Using a dynamic agent-based framework, Arthur [69] demonstrates that for technologies displaying increasing returns, the technology type which (perhaps by chance) "gains an early lead in adoption" can compound improvements over a longer time, leading competing technologies to become "locked out". Examples of technologies locked-in by increasing returns may include: the QWERTY keyboard, the narrowness of the British railway gauge, the National Television System Committee's 29.97 frames per second (in turn dependent on the locked-in 60 Hz power line frequency in North America), and the continued use of the FORTRAN programming language in scientific computing [69].

An economic regime showing path dependence possesses three properties closely related to chaotic systems' sensitive dependence on initial conditions: first, "non-predictability" where increasing returns "act to magnify chance events"; second, "inflexibility" where a dominant technology outcome becomes "progressively more 'locked in'" as adoption increases; and third, "non-ergodicity" where "historical 'small events' are not averaged away and 'forgotten' by the dynamics" [69]. In comparison to purely physical dynamical systems, however, economic path dependence can also carry a sense of normative loss or value judgement. Such a path-dependent economic process exhibits "potential inefficiency" where the increasing returns adoption process may result in "developing a technology that has inferior long-run potential" [69].

This uniquely normative aspect of inefficiency from economic path dependence raises a question of is-versus-ought distinction. Liebowitz and Margolis [70] differentiate between types of possible path dependence: first-degree path dependence does no harm (e.g. "a capricious decision to part one's hair on the left" may become locked in for life but leads to no health

detriments), second-degree path dependence leads to a path chosen using best available knowledge that "in retrospect" proves to be inferior, and third-degree path dependence leads to an "avoidable" inefficient outcome.

This notion of uncertainty that resolves as time progresses, inherent in the second-degree path dependence definition, is conceptually related to the concept of a regret function in decision theory and game theory [71]. Regret theory was originally proposed in [72] and [73] as a mechanism to explain apparent anomalies during decision making under uncertainty studied in behavioral science. Mathematically, regret quantifies this notion of an action being retrospectively better. More precisely, the regret function measures the difference between choosing an alternative i today compared to the optimal choice after seeing that the future will resolve to some state k; for example, the regret function can apply in terms of the costs of alternatives, where R can be some monotonically increasing function [74]:

$$Regret_{ik} = R\left(f_{ik} - f_k^{opt}\right)$$

Regret functions are commonly used to evaluate the performance of online estimation, such as machine learning algorithms, where uncertainty during a sequence of ongoing decisions may be resolved later and compared to static optimal choices [75]. Another application is to approach uncertainty in real-time optimization problems like robotics flight trajectory planning using regret functions [76]. This approach of comparing the "a-priori solution" to the "optimal solution, given the specific realization of the uncertain parameters" as in [76] can therefore be applied to quantify the extent of second or third-degree path dependence.

In addition to Arthur's increasing returns or network effects, sunk costs can also cause path dependence. Perhaps trivially, an economy inherits yesterday's durable capital stock, which represents endowments that affect today's investment or production decisions [70]. Specifically, a "firm with fixed assets will continue to use an inferior technology where the average variable costs of the old technology are lower than the average total costs of the new," leading the "inferior but still more profitable technology" to be locked in [70]. Balmann [77] reinforces the notion the locked-in effect, which is "an equilibrium that may be inefficient, but which can only be abandoned at extremely high costs," can occur even in the absence of increasing returns to scale or network externalities. This "locked-in situation" can be caused by the "time structure of necessary reinvestments and sunk costs cause the locked-in situation" [77].

In the macroeconomics literature, path dependence is sometimes called economic hysteresis, which can also be caused by sunk costs. To study the apparently lagged response of firms to exchange rate fluctuations, Dixit [78] formalizes a continuous-time model of real exchange rates as a Brownian motion, and characterize analytical bounds on the exchange rates that trigger firm entry or exit, calling this range of values a "band of inaction." Dixit's numerical results show that the width of this band of inaction increases with larger magnitudes of sunk costs and with greater volatility of the exchange rate stochastic process. Extending Dixit's theory of hysteresis, Baldwin [79] uses discrete-time dynamic programming (using Bellman's optimality principle to find the optimal control policy) to incorporate the firm's rational expectations over various autoregressive-moving average processes rather than just continuous time Brownian motion. Baldwin demonstrates the existence of economic hysteresis based on sunk costs, and also shows that the hysteresis band tends to increase in width as sunk costs

increase. This mechanism of economic hysteresis studied by Dixit and Baldwin does not depend on the existence of increasing returns to scale, since the marginal cost structure can be unaffected in spite of, or independently of, the sunk costs being already committed.

It is important to note that Liebowitz and Margolis attempt to categorize lock-in caused by sunk costs as "first-degree" or benign path dependence. Continued use of an existing asset that is "inferior but still more profitable" still maximizes economic social welfare, so Liebowitz and Margolis argue that this kind of lock-in effect never constitutes a market failure. In other words, under an efficient market, the "inferior" higher-variable-cost resource would have had a larger "discounted present value of the total social benefit" compared to the higher-capital-cost resource, so the continued locked-in usage is in fact desirable for society [70].

However, where this analysis breaks down is under an unaddressed market failure, such as an unpriced externality, in the static market. According to [70]'s definition the undesirable "third-degree" type of path dependence is "ex ante path inefficient," meaning that "at some time t_0 there is an alternative action a_1 such that the discounted present value of the total social benefit of selecting a_1 instead of a_0 are known to be greater than the discounted present value of costs, yet the action a_0 is taken." The crux of the issue is that knowledge about the relative costs and benefits does not necessarily translate to economic decisions consistent with this knowledge, if there are social externality costs not included in the private costs of agents making economic decisions. An old Chinese proverb states that it is easy to know but difficult to act. Using [70]'s framework, supposing there is no disagreement about the social discount rate, then at t_0 there is an action a_1 that is in sum socially superior to a_0:

$$NPV_{t_0}^{SB}(a_1) > NPV_{t_0}^{SB}(a_0)$$

What the authors' original claim ignores is that by definition if a_0 has negative externalities then the net private benefits exceed the net social benefits, in the absence of public policy:

$$NPV_{t_0}^{PB}(a_0) > NPV_{t_0}^{SB}(a_0)$$

Assume without loss of generality a_1 has no externalities, so $NPV_{t_0}^{SB}(a_1) = NPV_{t_0}^{PB}(a_1)$. While the presence of a negative externality does not guarantee that a_0's private net benefits exceeds a_1's, it is possible that such is the case. In a capitalist market economy, private firms make decisions based on their material, economic private costs and benefits, even if externalities are "known" by the firms. Thus, almost by definition, it is possible for third-degree path dependence a la [70] to occur under an unaddressed and sufficiently large negative externality, where the ex-ante "known" a_0 alternative is chosen by market forces:

$$NPV_{t_0}^{PB}(a_0) > NPV_{t_0}^{PB}(a_1)$$

This possibility means that while a negative externality is socially suboptimal in the static sense for every period of time that it remains unpriced, sunk costs might additionally cause lock-in, such that the negative externality could irreversibly persist even after a policy is enacted to internalize the economic externality. Philosophically, any investment decision made during the period of time after an externality is "known" (in a sense, fulfilling the *mens rea* legal test) – but before this externality is internalized by public policy such that private decisions are actually affected – can lead to capital investments with associated sunk costs and economic lock-in.

The line of reasoning about lock-in caused by simultaneous sunk cost and externality applies to greenhouse gas emission externalities. Erickson et al. in [5] investigate and quantify the existence of this particular mechanism of economic path dependence, termed carbon lock-in, in power generation and energy infrastructure assets. Carbon lock-in is defined as 'the dynamic whereby prior decisions relating to GHG-emitting technologies, infrastructure, practices, and their supporting networks constrain future paths, making it more challenging, even impossible, to subsequently pursue more optimal paths toward low-carbon objectives" [5]. The authors explicitly quantify the extent of carbon lock-in along the economic dimension by measuring the "financial barrier to unlocking," i.e. how high a future carbon price must be in order for the new renewable energy alternative to be competitive with an existing (sunk cost already incurred) fossil fuel source. In particular, [5] includes calculations for natural gas power generation plants, suggesting that "gas power may be over-built in the near term" but estimating that lock-in of gas power plants can be escaped with a carbon price of \$20 / ton CO_2.

In addition to the sunk cost mechanisms, many other factors can affect the existence and extent of carbon lock-in. The most straightforward is the duration of the equipment lifetime [5]. Unruh [6] also proposes the idea of a "Techno-Institutional Complex" where lock-in "occurs through combined interactions among technological systems and governing institutions," including organizational inertia in policies and business practices. In addition, the classic network externalities a la Arthur's analysis also apply to the vast networks of energy infrastructure, in terms of the positive feedback involved in the expansion of electric power grids [6] and the oil and gas supply pipelines [5]. For example, [80] argues that natural gas pipelines "lock-in demand and emission," and that development of "new pipelines will unlock a surge of fracked gas."

From an evolutionary economics perspective, Marechal [81] argues that in contrast to the mainstream economics literature, the presence of lock-in effects renders "traditional cost-efficient measures (such as carbon taxation or tradable emission rights) aimed at internalising external costs" to be insufficient at enabling "the required radical changes in the field of energy." This is a serious allegation that permanent technological lock-in can make externality pricing – the economist's preferred tool to deal with negative externalities – futile. More specifically, in "A Bridge Too Far: Building Off-Ramps on the Shale Gas Superhighway," Parenteau and Barnes [82] argue for more aggressive policy actions in order to "offset the 'path dependency' nature of investment in unconventional gas recovery."

Adding to possible concerns about natural gas development is the release of fugitive methane emissions in the supply chain of natural gas production. Methane CH_4 is several times more potent of a greenhouse gas than carbon dioxide CO_2; over a period of 20 years and including climate-carbon feedback effects methane has a global warming potential of 86 times that of carbon dioxide, according to the IPCC [3]. Ren et al. [83] use aircraft measurements to estimate the leakage rate from oil and natural gas operations in the Marcellus Shale region to have a mean of 3.9% with standard errors of 0.4%; this estimate is consistent with prior "top-down" studies based on direct chemical observations, but is higher than some "bottom-up" inventory-based studies that may depend on scaling assumptions.

Zhang et al. [84] quantify a margin of safety for natural gas to be a net benefiicial "bridge fuel", by calculating the maximum breakeven delay on zero-emission energy sources, i.e. "by how many years earlier or later natural gas energy system could alter the transition to a near-zero-emission energy system while providing an equivalent climate effect as the reference coal case." In a numerical example under assumptions including a 4% natural gas leakage rate, the authors calculate that switching from coal to a "natural gas energy system could delay introduction of near-zero emission energy systems by 24 years without losing all of the climate benefits of shifting from coal to natural gas" [84].

Overall the authors in [84] raise caution that "[i]f the introduction of natural gas substantially delays the transition to near-zero emission systems," then the switch to natural gas could cause "greater amounts of warming than would have occurred otherwise." It is important to keep in mind that [84] does not predict that such a delaying effect would necessarily occur or delineate the mechanisms for such a delay, instead the study only says that a limited amount of such a delay may still be compatible with natural gas being net beneficial as a bridge fuel.

Mignone et al. [7] specifically address the concerns that "reliance on natural gas in the early years of a national program to reduce power sector emissions could make it more challenging to meet longer-term emission reduction goals in the power sector, if those goals are significantly more stringent than nearer-term ones." The study looks at how robust natural gas combined cycle (NGCC) capacity buildout is to the increase in future levels of a carbon price; therefore, this framework is mathematically related to the carbon lock-in question from today's perspective (zero vs. carbon price today, compared with medium vs. high carbon price in the future). [7] directly applies the Electricity Market Module (EMM) within the National Energy Modeling System (NEMS) developed by the Energy Information Administration (EIA).

Table 1: Natural Gas Generation and Capacity in Optimal Solutions Under Capped and Rising Carbon Regulation Scenarios, from Mignone et al.

	Generation (TWh)			Capacity (GW)			Capacity Factor		
	2015	2030	2050	2015	2030	2050	2015	2030	2050
Capped Price	1092	1260	1753	226	277	386	55%	52%	52%
Rising Price		1328	1525		299	406		51%	43%

The results from [7] appear to contradict the existence of any lock-in effect predicted by Erickson et al., by implying that "anticipation of rising carbon prices does not deter near-term NGCC deployment relative to what it would have been without such anticipation." The authors of [7] provide an intuitive explanation for the results: "NGCC capacity is desirable for its capacity value – that is, its ability to provide energy during periods of time when generation from solar and wind resources is low." In fact, the numerical values show a still increasing trajectory in the optimal gas capacity under the case of more aggressive carbon pricing, at the same time that the average capacity factor decreases from 51% to 43%, suggesting that "NGCC benefits from its flexibility to partially shift between generation and capacity value streams over time in response to market and policy conditions" [7].

3. Data Analysis

3.1 Data Methodology

Historical hourly-resolution values over 6 years of 2007 to 2012 of intermittent renewable energy and load demand are used. These years are chosen because of limitations of available wind power data, and the time periods of the solar and load data are chosen to match those of wind. All the studies surveyed in the literature review that use hourly resolution load balancing match the time index of intermittent generation with intermittent load. Since the common weather random variable creates temporal correlations between load and variable renewable generation, the empirical datasets for these sourced should be synchronized in each time period.

3.1.1 Hourly Wind Data

The National Renewable Energy Laboratory (NREL) publishes the Wind Integration National Dataset (WIND) Toolkit. Within this dataset, the Techno-Economic WIND Toolkit contains 5-minute and coarser temporal resolution data for 6 years (2007 – 2012), and can be accessed via a web API that returns CSV or JSON files [85]. NREL calculates each location's wind power data based on applying meteorological data for each 2-km by 2-km grid cell to assumed turbine power curves. Draxi et al. [86] provide a full documentation of this calculation methodology and model validation.

Metadata descriptions for each of the 126,000 individual sites are accessed via a CSV file from the "WIND Toolkit Power Data Site Index" [87]. Each site has longitude and latitude coordinates and the megawatt nameplate capacity. Filtering for only the six states that are almost entirely within PJM (Ohio, Pennsylvania, Virginia, West Virginia, Maryland, New Jersey), there are 6,110 individual wind sites. Using this metadata, a Python script is written to query the above Wind Toolkit Data API using well-known text (WKT) geospatial strings. The power output data values are normalized by the specific location's assumed nameplate capacity given in the metadata, to produce hourly available capacity factor data in terms of percentages.

3.1.2 Hourly Solar Data

As of the time of writing this paper, the available NREL solar power dataset comparable to the wind toolkit only contains data for 2006, which does not temporally match the wind years. NREL is currently working on developing a solar toolkit (SIND) that will be comparable to that for wind, but this is not yet available [88]. The "Solar Power Data for Integration Studies" dataset contains synthetic solar photovoltaic power plant data in the format of CSV [89]. The site coordinates of this dataset is used to assume locations that have been vetted as reasonably plausible in terms of physical, environmental, or other siting constraints.

Solar power production data values for 2007 to 20012 are synthesized using NREL's software development kit and System Advisor Model (SAM) version 2017-1-17 using the Python interface. The SAM solar module requires several user-specified inputs. The system's

DC / AC ratio is the ratio of the solar module capacity versus the power output of the inverter module. This ratio is assumed to be 1.2 (i.e. the solar panel module has a maximum output greater than that of the power control electronics, which can lead to output "clipping" at high solar times), which is in line with optimal values in industry recommendations [90][91]. The efficiency of the inverter (defined as the AC power output divided by the DC power input, both measured in watts) is assumed to be 95%, which is also in line with industry values [92][93]. All solar sites are assumed to have two-axis trackers, i.e. the solar panels are assumed to be tracking the sun's azimuth as well as tilt angles, which maximizes the available solar output for a given amount of installed solar capacity. The output is verified to check that the output power scales linearly with the system capacity input parameter, so setting capacity to 1 MW would give numerical values equal to the desired capacity value percentage for each given hour.

For simplicity during data loading, solar and wind generation data are compiled for the seven states with entirety or near entirety of land area within PJM: PA, NJ, MD, DE, VA, WV, OH. This rule leaves out some portions of the PJM footprint, i.e. the north of Illinois and east of Kentucky. The following table summarizes the total number of individual renewable energy sites for solar and wind.

Table 2: Number of Data Series Sites Loaded

State	Area (Square Miles)	Solar sites	Wind sites
PA	46,055	101	1,428
NJ	8,729	100	326
MD	12,407	80	271
DE	1,981	16	111
VA	42,775	221	481
WV	24,038	24	542
OH	44,825	95	3,061

3.1.3 Hourly Load Demand Data

PJM publishes hourly-resolution data for metered net load (measured in MWh, which corresponds to an average power output MW with the same numerical value) within the PJM regional transmission operator (RTO) footprint, from 1993 onwards, and can be accessed via CSV files [94]. The data quality for this source is very robust because this represents an aggregation of actual ground truth load energy data used for billing purposes. Data for individual load zones are available, but the total RTO-level values are used.

3.2 Dimensionality Reduction with Quadratic Programming

The literature on intermittent renewables clearly show a diversification effect from aggregating different geographical locations. Moreover, having fewer distinct resource types translates to lower dimension in the load balance and other constraints for later optimization analysis. Therefore, some form of statistical averaging should be performed on the several thousand individual renewable energy sites (each with hourly resolution for six years), which can be interpreted as a dimensionality reduction step to aid later analysis.

The simplest averaging is an arithmetic sum, and represents an equal-weighted portfolio of each of the listed geographical sites found in the metadata. Thinking in terms of portfolios, a more sophisticated averaging algorithm to mitigate the detrimental effects of intermittency might be based on Markowitz mean-variance optimization. Given portfolio weights w, the portfolio-level returns are $w^T m$ and portfolio variance is $w^T \Sigma w$, where Σ is the variance-covariance matrix [91]. If short-selling is allowed, i.e. there can be a negative amount allocated to a particular asset, then the optimal mean-variance optimum can be analytically solved when parametrized by a risk-return tradeoff λ that is mathematically a Lagrange multiplier [95].

However, power generation cannot physically be sold short. The problem requires nonnegativity constraints, and thus requires numerical optimization. Since the variance objective is quadratic in terms of the decision variable weights, a quadratic programming (QP) problem can be formulated:

$$\begin{aligned}
&\text{minimize } \tfrac{1}{2} w^T \Sigma w && \text{(Minimize portfolio variance)}\\
&\text{subject to } w^T m \geq r && \text{(Target returns)}\\
&\qquad \mathbf{1}^T w = 1 && \text{(Sum of weights)}\\
&\qquad \mathbf{0} \leq w \leq \mathbf{1} && \text{(No short-selling)}
\end{aligned}$$

The Python Pandas library is used to compute the covariance matrix Σ of both hourly and daily-grouped capacity values for the 607 solar sites, i.e. the covariance matrix has dimension (607×607). Then the QP is implemented, to target r to be at least the average capacity factor of the equal-weighted mean, and solved using MATLAB with the standard solver utilizing an interior point algorithm. The following table shows that optimizing on hourly values reduces hourly standard deviation (i.e. variability in the intermittency decomposition) compared to equal-weighted by 2.59% in terms of nominal values, while optimizing on daily values reduces daily standard deviation by 9.83%.

Table 3: Comparison of Max, Mean, and Mean-Variance Optimized Solar Portfolios

	Max individual (1168024)	Equal Weight Mean	Min Hourly Var	Min Daily Var
Mean	25.00	22.63	22.63	23.01
Hourly Std	33.30	28.16	27.43	28.00
Daily Mean Std	10.65	9.26	8.57	8.35

Another analysis to visualize the effect of aggregation on reducing intermittency is to

simply sample incrementally larger samples (here the sites are ranked by capacity values), and calculating the sample standard deviation based on an equal-weighting for each iteration.

Figure 2: Hourly (Left) and Daily (Right) Standard Deviation, for Equal-Weighted Portfolios at Different Numbers of Solar Sites Included (Ranked by Capacity Value)

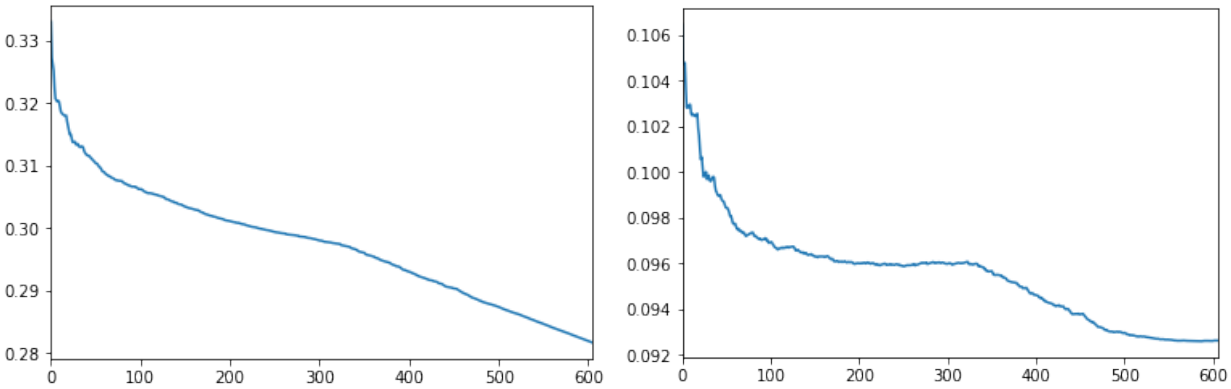

The same procedure is repeated for the much larger wind series dataset, resulting in a $(6{,}220 \times 6{,}220)$ variance-covariance matrix. In the following table, using hourly-level optimization reduces portfolio hourly standard deviation by 19.67%, while daily-level optimization results in a 23% reduction in daily standard deviation, compared to the equal-weighted mean.

Table 4: Comparison of Max, Mean, and Mean-Variance Optimized Solar Portfolios

	Max individual (45372)	Equal Weight Mean	Min Hourly Var	Min Daily Var
Mean	59.62	42.01	42.01	42.01
Hourly Std	39.06	25.93	20.83	20.95
Daily Mean Std	31.40	22.67	18.04	17.50

Figure 3: Hourly (Left) and Daily (Right) Standard Deviation, for Equal-Weighted Portfolios at Different Numbers of Wind Sites Included (Ranked by Capacity Value)

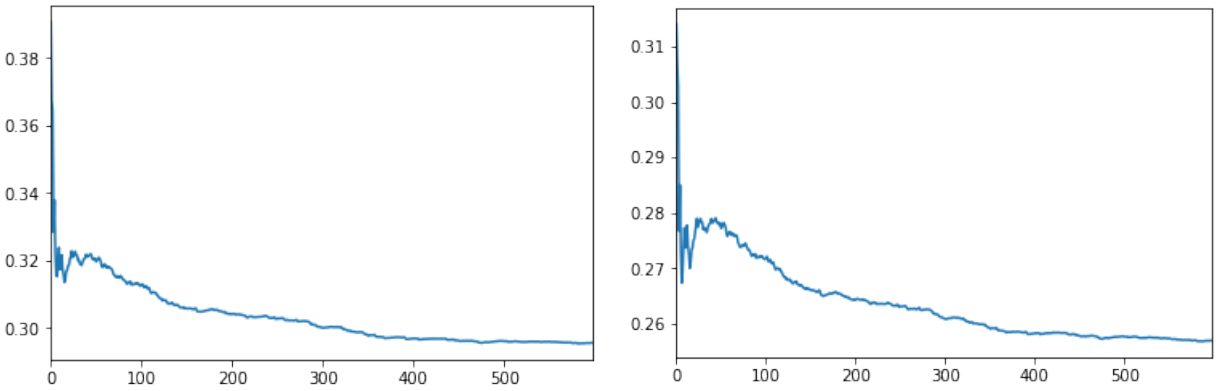

Evidently the amount of variability reduction that can possibly be achieved with the ex-

post, in-sample optimization appears greater for wind power than for solar power. This observation is consistent with the literature on renewables intermittency. Intuitively, high-level solar output is primarily driven by the motion of the sun in the sky, so more strategically aggregating solar plants that are all situated in the mid-Atlantic states of PJM will have limited improvement (though clearly not zero) in the diversification effect. In other words, picking and choosing the best risk-adjusted solar sites would not reduce overall variability as much as picking and choosing wind sites.

It is important to note two major limitations of this quadratic programming method. First, the actual objective function in a power systems context would be more akin to something like maximizing the energy portfolio's correlation with load demand, rather than a non-discriminating preference to lower variance across all times. Specifically, the actual impacts on grid integration costs are not fully captured by just the standard deviations; higher moments of the statistical distribution including time correlations with load have a large effect.

Second, the above mean-variance optimization uses in-sample data, in the form of mean capacity values for each site and their covariance matrix, to find the minimum variance portfolio of wind or solar sites that achieves the same average capacity value as the simple mean portfolio. The more parsimonious assumption of just using simple average may still be preferable. Using in-sample data may bias the amount of possible variance reduction available versus for a future unknown period. In addition, holding equipment efficiency constant, in reality the system's capacity value from wind or solar is likely to reduce over time because the highest-capacity resource sites would tend to be developed first. Moreover, in reality there is no existing mechanism that globally optimizes the renewable energy siting decisions based on system grid integration costs; siting decisions by renewables developers is determined by financial (e.g. expectations of electricity market conditions) and regulatory factors.

Conversely, the fact that the actual objective function in a capacity expansion optimization does not directly use renewable energy variance means that the quadratic programming approach for dimensionality reduction can still be useful. The above results suggest that the difference is likely not large for solar power, and so both the equal-weighted and mean-variance optimized wind data series could be analyzed.

3.3 Time Series Descriptive Statistics

The PJM load data series, plotted below, exhibits very strong seasonality patterns. A simple linear regression (OLS) model including a second-order polynomial of days and seasonal dummy variables for month, day of week, and hour of day has an adjusted R^2 of 0.6633, implying a large amount of the variation in electricity load demand can be explained by seasonal structures alone.

Figure 4: PJM-Wide Load Demand

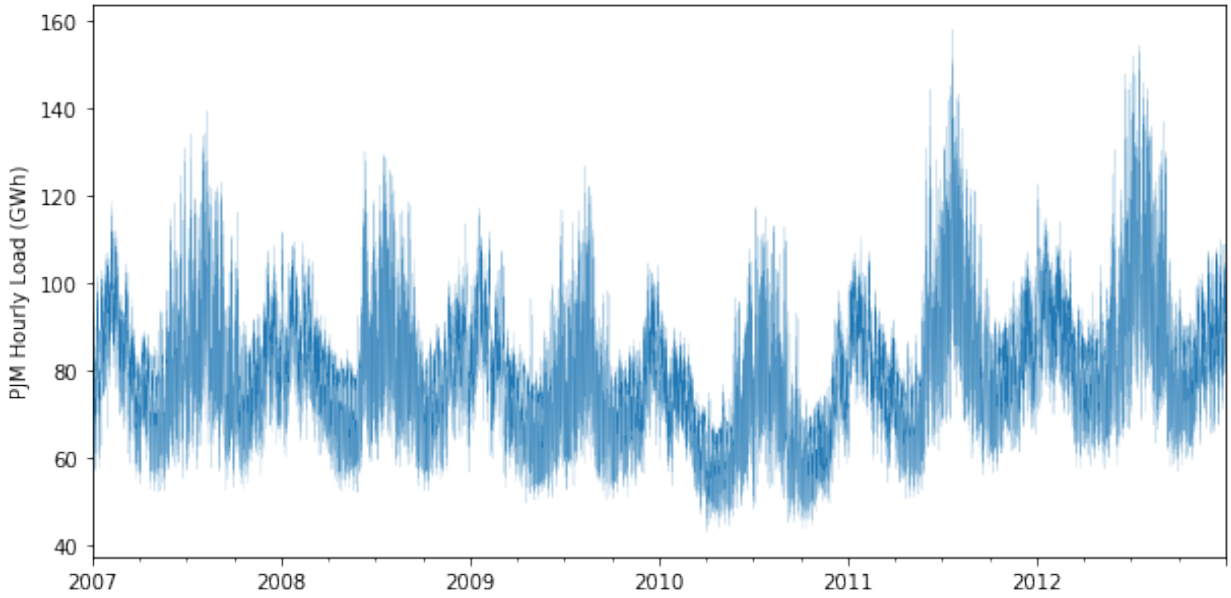

To better visualize the seasonality structure, the residuals after removing the polynomial time trend are averaged across month and hour groupings, which are plotted below. The left plot below shows that within an annual cycle, PJM load demand exhibits two peaks: a peak in the winter months most likely resulting from heating usage, and a larger peak in the summer months most likely resulting from air conditioner usage. The right plot below shows that within a daily cycle, load demand starts to increase in the early morning and persists (corresponding to the workday) then decreases towards nighttime when most of the population sleeps.

Figure 5: Annual and Diurnal Seasonality in PJM Load Demand (De-Trended)

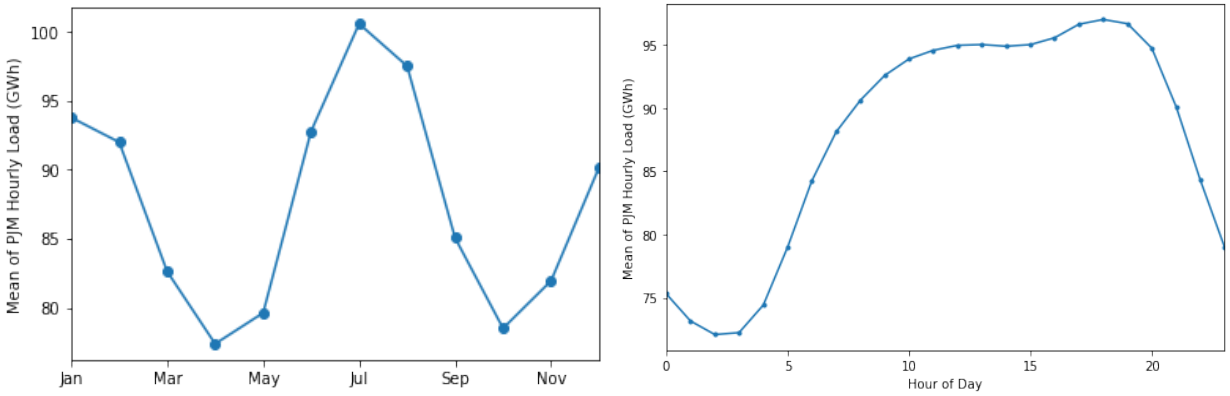

There are interactions between different seasonal components, as seen in the plots below. The left plot shows how the diurnal load profile changes between seasons. For example, the winter months exhibit a strong bimodal pattern, not seen in the other seasons. Further, the right plot shows that the load demand on weekends tends to not just be lower in level but also appears to be slightly lagged, compared to demand on weekdays on average. The complex seasonal structure highlights the need for datasets to be synchronized temporally for accuracy.

Figure 6: Interactions of Diurnal Seasonality with Annual and Weekly Patterns

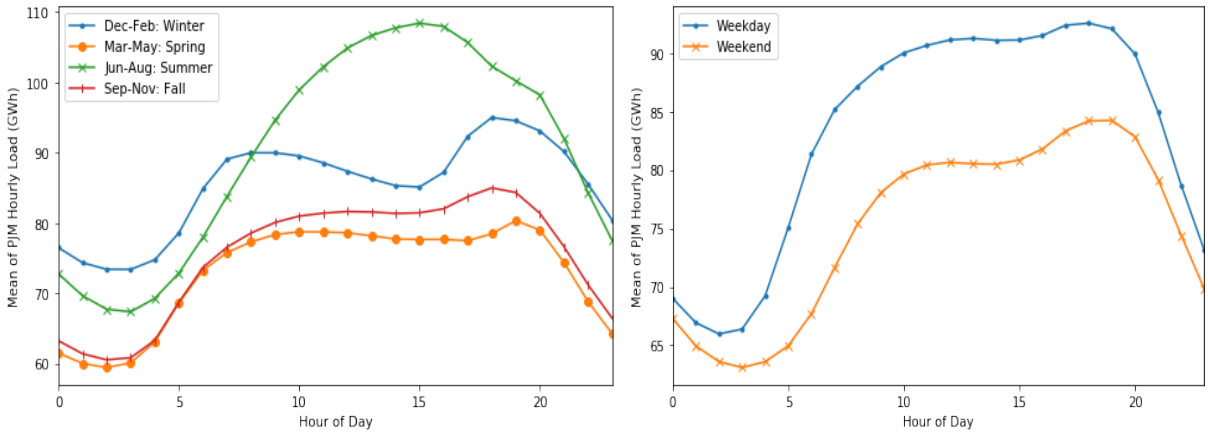

4. Analytical Framework for Lock-In

The purpose of this analytical section is to develop a bottom-up rigorous understanding of the economic path dependence mechanism, by incrementally layering complexities on deliberately simplified frameworks. The simplifications here help to highlight the most salient mathematical features of carbon lock-in's conditions and properties. By developing intuition and foundational understanding of the characteristic ways that carbon lock-in can manifest, later results using numerical optimization modeling can be better interpreted and understood – rather than simply treated as output from a black-box model.

4.1 Lock-In Range: Energy Substitution

This section extends the work of Erickson et al. by considering the more nuanced question of what conditions on the carbon externality cost would produce lock-in, as well as the effects of other economic parameters. The approach is intended to be agnostic between different regulatory environments, e.g. cost of service versus competitive markets, in line with the earlier discussion about optimality versus market outcomes; however, in practice institutional structures such as capacity markets may meaningfully change the outcomes compares to these ideal approximations.

In a generalized framework, economic path dependency can occur for investment decisions because any sunk costs made in a previous period (by definition of being sunk) cannot affect the optimality of decisions in subsequent periods. Consider an abstract generalized framework, in a simple setting with two periods of investment decisions. Suppose there are just two resource types, A and B. For this section assume that these resources are perfectly substitutable in terms of reliability constraints and ancillary services; this substitutability assumption will be examined explicitly in a later section.

Let I_A, I_B represent capital costs for two resources in providing substitutable services, and O_A, O_B are their total operating costs scaled properly to account for intertemporal tradeoffs, i.e. time discounting. A new operating cost C_A represents an economic externality, or a future increase to operating costs, which is only experienced by the "conventional" resource A. Since these are economic costs, $I_A, I_B, O_A, O_B, C_A \geq 0 \in \mathbb{R}$. The question is: when will the "alternative" resource B will be economically locked-out?

Three necessary and sufficient conditions would characterize a lock-in situation:

1. "Additionality 1": The absence of the externality cost renders resource A to be cheaper and thus preferred. In the absence of this condition, then there would never be new investments in A; conversely, the "alternative" resource B would always be preferred even without considering externalities.

$$V_{A,new}^{private} < V_{B,new}$$
$$\Rightarrow I_A + O_A < I_B + O_B$$

2. "Additionality 2": The inclusion of the externality cost flips the preference of investment. In other words, the externality cost is high enough such that resource B is now more economical. In the absence of this condition, resource B is not economical regardless of

whether or not there are already-constructed assets of type A that exist.

$$V_{A,new}^{social} > V_{B,new}$$
$$\Rightarrow I_A + O_A + C_A > I_B + O_B$$

3. "Lock-out": Existing units of resource A is cheaper to operate than new units of resource B, even when the externality cost is now included. The crux of this condition is that the cost to operate an existing resource A unit does not include any capital investment costs.

$$V_{A,old}^{social} < V_{B,new}$$
$$\Rightarrow O_A + C_A < I_B + O_B$$

Together these three conditions can be summarized to a range condition on the relative magnitude of C_A, compared to the other cost parameters, which leads lock-in to exist:

$$0 < I_B + O_B - O_A - I_A < C_A < I_B + O_B - O_A$$

Intuitively, for lock-in to exist the true externality cost cannot be too high, otherwise its inclusion would render irrelevant the existence of already-existing assets, with sunk costs worth I_A. Conversely, the true externality cost cannot be too low, otherwise its inclusion even during the initial investment period would not have led to investments in the resource B alternative. The width of this range is just I_A, consistent with the intuition that the larger the capital costs are relative to operating costs, the more likely there is to be a lock-in effect.

Consider again the specific carbon externality setting, to explicitly write the above algebraic expressions to account for the abovementioned intertemporal tradeoff scaling, i.e. discounting. The main limitation of the Erickson et al. framework is that it only considers the "lock-out" condition by calculating the equilibrium between existing dirty energy and new clean energy. Therefore, [1] implies that carbon lock-in exists for any level of an imposed carbon price that is lower than this equilibrium point; intuitively if this carbon price representing a true belief about the social cost of carbon is low enough then the alternative renewable resource would not have been preferred in the counterfactual initial period. In other words, [1]'s calculations do not account for the first two additionality conditions.

The framework is that the energy resource with a lower energy-normalized present value of production costs, i.e. levelized cost of electricity (LCOE), is chosen. In the notation of [1], the levelized cost is:

$$LCOE = \frac{\left[I + \left(\frac{O+F+C}{r}\right)\left(1 - \left(\frac{1}{1+r}\right)^n\right)\right]}{\frac{E}{r}\left(1 - \left(\frac{1}{1+r}\right)^n\right)} = \frac{[I + (O+F+C)D]}{ED}$$

Where the discount factor $D = \frac{1}{r}\left(1 - \left(\frac{1}{1+r}\right)^n\right)$ relates a stream of annuity payments to the present value. I is capital investment, O is operating and maintenance cost, F is the fuel cost, and C is the carbon price payment. The average annual energy generation is (ignoring leap days for simplicity):

$$E = (MW\ capacity)(\%\ average\ capacity\ factor)(8760\ hours)$$

Assume that the alternative resource is more expensive in the absence of a carbon price, i.e. the first additionality condition above is trivially satisfied. Also assume that the clean resource has no fuel costs, which is valid for wind and solar PV. Then the other two conditions of additionality and lock-out, expressed in terms of LCOE, are:

$$LCOE_{dirty,new} > LCOE_{clean,new}$$
$$LCOE_{dirty,old} < LCOE_{clean,new}$$

$$\frac{[I_d + (O_d + F_d + C_d)D_d]}{E_d D_d} > \frac{[I_c + O_c D_c]}{E_c D_c}$$
$$\frac{(O_d + F_d + C_d)D_d}{E_d D_d} < \frac{[I_c + O_c D_c]}{E_c D_c}$$

Simple rearranging gives a range of true carbon prices, whose delay will lead to carbon lock-in:

$$C_d > \left(\frac{E_d}{E_c}\right)\frac{I_c}{D_c} + \left(\frac{E_d}{E_c}\right)O_c - O_d - F_d - \frac{I_d}{D_d}$$
$$C_d < \left(\frac{E_d}{E_c}\right)\frac{I_c}{D_c} + \left(\frac{E_d}{E_c}\right)O_c - O_d - F_d$$

Assuming the fixed financial cost parameters, the carbon lock-in range has a width equal to:

$$\frac{I_d}{D_d} = \frac{I_d r}{\left(1 - \left(\frac{1}{1+r}\right)^n\right)}$$

An interpretation is that for larger values of the dirty energy source's capital cost, equipment duration, or discount rate, the range is larger larger for possible values of the pollution externality that can create a lock-in effect. The intuition of the first inequality is that the true carbon price cannot be too low such that even a new dirty plant is still more economical. The intuition of the second inequality is that the true "believed" carbon price cannot be too high such that even an existing dirty plant is not economical.

For numerical illustration, consider the case of natural gas and wind, using Erickson et al.'s cost parameters, $r = 10\%$ (which can represent a weighted average cost of capital), with natural gas power lasting 30 years and wind lasting 25 years. Natural gas is assumed to have an emissions rate of 0.79 tons CO_2 / MWh. These particular values are intended to illustrate the carbon price lock-in range concept, as well as provide a comparison to the point estimate in the original paper. More realistic and updated values are used for the later empirical section; for example, a state-of-the-art combined-cycle gas plant is much more efficient in terms of heat rate than the assumptions used here for illustration.

Under this example with a $50 per ton true externality price, carbon lock-in clearly exists. When the carbon price is included, wind investment would occur because it is cheaper to build new wind ($85.93 / MWh) compared to new gas ($100.58 / MWh) for the same energy generation. However, if there are already-existing gas assets, resulting from earlier investments during a time when the full carbon costs were not included, then it is cheaper to continue using this extant gas ($79.02 / MWh) than build new wind.

Table 5: Example Levelized Cost of Electricity Calculation (LCOE)
Comparing New vs. Existing, Gas vs. Wind. Assuming $50 / ton carbon dioxide price.
These are intended for illustration, not actual results.

	Gas	Wind	
Investment (**I**)	730	1500	$
Lifetime (n)	30	25	Years
Discount rate (r)	10%	10%	
Discount factor (**D**)	9.43	9.08	
Capacity factor	0.41	0.27	kWh/kW
O&M cost (**O**)	23	38	$ / Year
Emission rate	0.79	0	T CO2 / MWh
Plant Capacity	1	1	kW
Energy (**E**)	3.59	2.37	MWh/ Year
Fuel price	9.2	0	$ / GJ
Fuel cost (**F**)	118.95	0	$ / Year
Carbon price	50	50	$ / T CO2
Carbon cost (**C**)	141.87	0.00	$ / Year
LCOE (New)	**100.58**	**85.93**	$ / MWh
LCOE (Existing)	**79.02**	**16.07**	$ / MWh

Furthermore, while a $50 price results in lock-in, the above framework can be used to analytically find the entire range of carbon prices producing lock-in. Using the above parameters and simplified algebraic inequalities for C_d, the range of true carbon prices (measured in dollars per ton of carbon dioxide) that achieves carbon lock-in can be easily calculated. These are, after adjusting for the total emissions volume:

$$\$31.46 < \frac{C_d}{r_{emm} \cdot E_d} < \$58.75$$

The below plots show sensitivities for select variables, with other variables held constant at the base case, in order to visualize the effect on the range of carbon prices inducing lock-in. Decreasing gas capital cost means a much higher true carbon price in order for lock-in to occur, by narrowing the band of prices compatible with lock-in. Conversely, decreasing wind capital cost leads to a decrease in the level of the lock-in range, without affecting the interval width. Decreasing natural gas fuel cost has the opposite effect, by raising the carbon prices required for lock-in. The higher the discount rate or required rate of return, i.e. the less future economic value matters relative to today's value, the higher the minimum required carbon price for lock-in is; however, an increased discount rate also increased the width of the range of lock-in compatible carbon prices.

Figure 7: Carbon Lock-In Ranges' Upper and Lower Bounds, as Functions of Cost Parameters

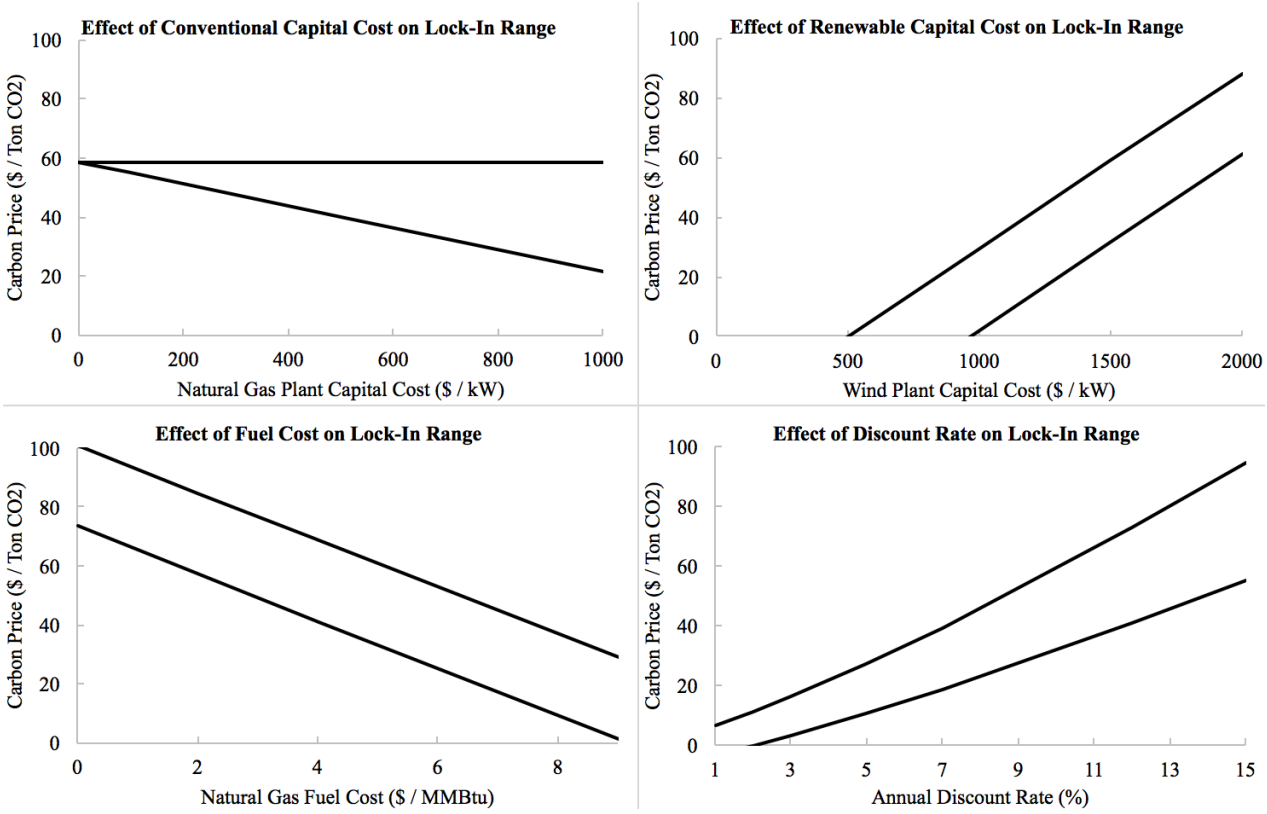

The main novelty from this section is that whereas the original framework would have been able to trace out these sensitivities for the upper bound of the carbon lock-in range, the original binary framework also would predict the existence of carbon lock-in for all lower values of the carbon price. In contrast, this section develops the concept of a carbon lock-in range similar to the "band of inaction" of [78], by also establishing a lower bound for lock-in compatible carbon prices. Over the space of possible beliefs on the true social cost of carbon, therefore, this new analytical framework serves to decrease the feasible area where lock-in could occur.

4.2 Load Intermittency: Load Duration Analysis

The above analysis based on LCOE alone fails to account for the time nature of variability in electricity demand. A common industry analysis tool is the load duration curve, which can be constructed by sorting in descending order each hour's load demand by magnitude. The resulting duration curve is mathematically equivalent to the inverse cumulative distribution function or CDF [96]. The sorting can be interpreted as a transformation from the chronological time domain to the probability space. Specifically, the load duration curve function can be interpreted mechanistically from the sample distribution or probabilistically from an underlying population of electric demand:

$$f^{-1}(l) = P(load \geq l)$$

Figure 8: Load Duration Curve for PJM, Constructed by Sorting Hourly Demand

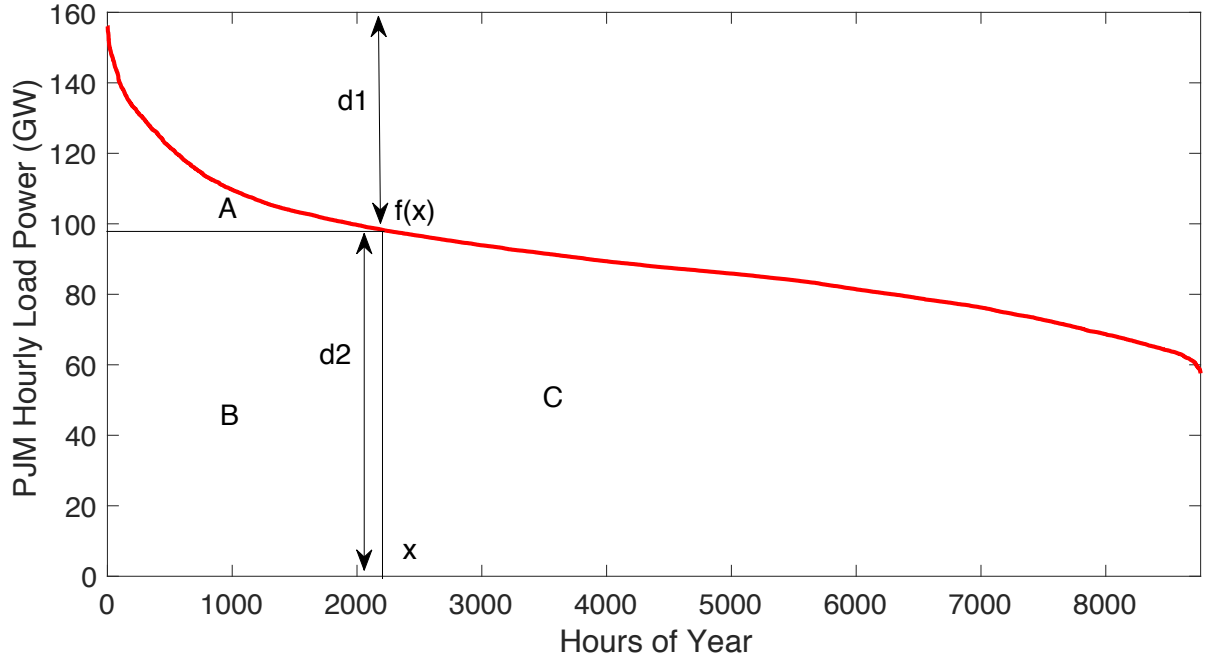

Suppose the load duration curve can be described analytically as a continuous, once-differentiable function, which appears reasonable given the smooth shape seen above in the empirical data. By definition, energy is time integral of power or $E = \int_0^T p(t)dt$, and so corresponds to area in the diagram.

Without loss of generality, the total cost for a given mix of resource 1 covering the x top hours of the year and resource 2 acting to serve "baseload" will consist of properly time-discounted capital costs and variable energy costs – abstracting away from other operational constraints and costs. Corresponding to the vertical axis in the diagram above, there must be enough resource 2 capacity to cover up to $f(x)$, after which resource 1 will enter the dispatch and so there must be $f(0) - f(x)$ of resource 1 to cover the maximum hour load. The time integral $\int_0^x f(s)ds$ corresponds to regions A plus B, while region B is the rectangle with area $xf(x)$, and finally region C corresponds to the integral $\int_x^{x_{max}} f(s)ds$. Thus the total cost

function for each mix, parametrized by the amount of load coverage of resource 1, can be written as:

$$\begin{aligned} J &= k_1 d1 + k_2 d_2 + v_1 A + v_2 (B + C) \\ &= k_1 [f(0) - f(x)] + k_2 f(x) + v_1 \left[\int_0^x f(s) ds - x f(x) \right] + v_2 \left[\int_x^{x_{max}} f(s) ds + x f(x) \right] \end{aligned}$$

Find the first order condition, which will give globally optimal solution if the cost function is convex, by applying second fundamental theorem of calculus:

$$\begin{aligned} \frac{\partial J}{\partial x} &= -k_1 \frac{\partial f(x)}{\partial x} + k_2 \frac{\partial f(x)}{\partial x} + v_1 \left[f(x) - f(x) - x \frac{\partial f(x)}{\partial x} \right] + v_2 \left[-f(x) + f(x) + x \frac{\partial f(x)}{\partial x} \right] \\ &= (k_2 - k_1) \frac{\partial f(x)}{\partial x} + (v_2 - v_1) x^* \frac{\partial f(x)}{\partial x} = 0 \end{aligned}$$

Assuming $\frac{\partial f(x)}{\partial x} \neq 0$, which is economically reasonable since by construction the load duration curve is monotonically decreasing, the optimal capacity mix for the case of two perfectly dispatchable resources (an assumption that will later be examined) can be found analytically by dividing both sides by the first derivative terms:

$$x^* = -\left(\frac{k_2 - k_1}{v_2 - v_1} \right) = \frac{k_2 - k_1}{v_1 - v_2}$$

This x^* implies an optimal level of resource 1 is $f(0) - f(x^*)$, and for resource 2 is $f(x^*)$. This is a feasible solution, i.e. time coverage $x^* \geq 0$ as long as $k_2 - k_1$ and $v_1 - v_2$ have different signs, which occurs whenever each resource does not strictly dominate the other one on both capacity and energy costs (one has to be cheaper in terms of capacity, and the other cheaper in terms of energy, in order for gains from trade to exist).

Without loss of generality, let $k_1 < k_2, v_1 > v_2$. In other words, let resource 2 be the more expensive but more efficient power plant. A concrete example is that a natural gas combustion turbine (CT) plant is easier to construct, and has lower capital costs, than a combined-cycle (CC) plant which combines a combustion turbine cycle with a steam turbine; conversely the CC plant is more efficient and has lower variable cost per unit energy than the CT plant.

Building on this analytical framework and closed-form solution for the optimal mix, the effect of path dependence can be determined in the more realistic dynamic load setting. Suppose there is some pre-existing capacity of resource 1 that does not exceed the above optimal amounts, $\theta_1 < f(0) - f(x^*)$, and $\theta_1 < f(x^*)$. The cost function is identical except the amount of capacity level for which new capital costs are incurred is now decreased; the energy variable costs are unchanged because the existing resources still need to incur variable costs.

$$J_{pre} = k_1[f(0) - f(x) - \theta_1] + k_2[f(x) - \theta_2] + v_1\left[\int_0^x f(s)ds - xf(x)\right] + v_2\left[\int_x^{x_{max}} f(s)ds + xf(x)\right]$$

Here the sunk costs of θ_1 and θ_2 are constants that do not depend on the chosen x, i.e. $\frac{\partial \theta_1}{\partial x} = \frac{\partial \theta_2}{\partial x} = 0$, so the first order condition's derivative is unchanged from before. In other words, any pre-existing capacity (or already-incurred sunk costs) that does not exceed the original optimal level does not lead to any path-dependent interference, because that amount of capacity is still useful and will be included in the optimal solution.

However, consider the extreme case when $\theta_1 \gg f(0) - f(x^*)$, meaning no capital cost for resource 1 needs to be incurred up until a larger x such that $f(0) - f(x^*) > \theta_1$. In this region of no capital cost, the first order condition becomes:

$$k_2 \frac{\partial f(x)}{\partial x} + (v_2 - v_1)x \frac{\partial f(x)}{\partial x} = 0$$

Therefore, the optimal mix is now given by:

$$x^{*(1)} = \frac{k_2}{v_1 - v_2}$$

By symmetry, if there is extra resource 2 exceeding the original optimal, $\theta_2 > f(x^*)$, then the optimal mix is given by the following. However, this possibility is not the focus because the idea of carbon lock-in corresponds to having too much of resource type 1 investment.

$$x^{*(2)} = \frac{k_1}{v_1 - v_2}$$

The implication of these analytical results is that excessive amounts of resource 1 will result in new $x^{*(1)} > x^*$, because $k_2 > k_2 - k_1$. The new optimal amount of resource 2 is now decreased compared to the counterfactual without this pre-existing capacity of resource 1, or $f\left(x^{*(1)}\right) < f(x^*)$, because the load duration curve is decreasing by construction. The exact magnitude of this amount of "locked-out" capacity is proportional to $\frac{k_1}{v_1 - v_2}$. Intuitively, the path dependence effect increases if the sunk cost of the already-committed resource is larger, but the path dependence effect diminishes as the new resource 2 becomes relatively cheaper in terms of variable costs. The exact translation of these relative directions translate to capacity levels is not linear because of nonlinearities in the load duration curve function.

Consider a numerical illustration. Let $k_1 = k_{CT} = 70, k_2 = k_{CC} = 120$ in \$ / kW represent capital costs scaled to annuity magnitudes, and $v_1 = v_{CT} = 50, v_2 = v_{CC} = 25$ in \$ / MWh represent operating costs. Then the optimal solution with no existing capacities will be the following:

$$x^* = \frac{100 - 70\ \left(\frac{\$}{kW}\right)}{50 - 25\ \left(\frac{\$}{MWh}\right)} = \frac{30}{25}\ (10^3 hr) = 1{,}200\ hr$$

This corresponds to the 1,200th hour in the load duration curve, or 106.76 GW. So the optimal mix starting from no pre-existing capacities consists of $f(0) - f(x^*) = 156.17 - 106.76 = 49.41$ GW of CT gas acting as "peaker" plants, along with 106.76 GW of CC gas.

Instead, suppose there already is substantially more than 50 GW of CT gas capacity, say 70 GW. Now $x^{*(1)} = \frac{100}{25} = 4{,}000\ hr$, corresponding to 89.38 of CC gas. This means the presence or sunk cost nature of the existing CT gas resources have locked-out 106.76 – 89.38 = 17.38 GW of CC capacity, clearly demonstrating the existence of path dependence. In turn, this translates to an amount of locked-out energy generation. Estimate the area integral as the sample sum up to the desired hour levels, to find the approximate corresponding energy generation share. If x is the hour number, then the discretized integral is:

$$E = xf(x) + \sum_{i=x}^{x_{max}} f(i)$$

Table 6: Numerical Illustration of Path Dependency Using Closed-Form Framework

Pre-Existing CT Capacity (GW)	Optimal Time Covered by CT (%)	Optimal CC Capacity (GW)	Optimal CC Share (%)
0	13.7	106.8	97.79
70	45.7	89.4	92.58

These results were identical to those obtained from an LP formulation of the same problem, as long as the pre-existing capacity is sufficiently large, verifying the validity of the simple closed-form solution.

4.3 Renewables Intermittency: Capacity Substitution

Simply considering the energy generation substitution between resource types ignores the intermittent nature of variable renewable generation via wind turbines and solar photovoltaics. Since load demand is empirically never zero, the presence of near-zero renewable generation hours means the system requires some dispatchable "backup" units to provide power capacity in order to satisfy resource adequacy. Energy storage and demand shifting resources play part of this backup role, and their inclusion on the system may increase the degree of possible substitution.

Power capacity (MW) substitution is crucial to assessing carbon lock-in because energy generation has very time-dependent value due to electricity usage's strong seasonality structure. If dispatchable capacity is still required due to the lack of perfect substitution, even under the scenario with full externality accounting, then lock-in cannot be said to occur. In other words, any initial new investments in the dispatchable capacity is still useful, independent of whether externality prices are incorporated.

This section will explore to what extent additions of alternative power capacity can substitute the need for dispatchable capacity. The focus is on the extent of technical substitution, so economic costs are not discussed in this section. In reality, just because a resource can technically substitute away another does not mean it is economic to do so; in the later empirical optimization section this tradeoff will be explicitly considered.

For clarity of illustration, the simplified case of just one variable renewable energy source (wind or solar) and one dispatchable source will be considered. As well, only hourly resource adequacy will be considered, i.e. operational constraints will be ignored for simplicity. The practical limitations arising from these simplifying assumptions include the fact that operational constraints, such as the need for various contingency reserves, may increase at higher levels of renewables usage as the impact of renewable forecast uncertainty increases.

4.3.1 No Storage or Demand Response

Under the simple case of no storage and perfectly inelastic demand, the required generation dispatch is determined once given the renewable and load vectors. Ignoring operational constraints, the least cost generation dispatch will utilize all the available variable power (trivially, the solution with minimal dispatchable capacity will also maximize renewable usage), then the remaining net load "NL" will have to be met by the dispatchable resource. Then the required dispatchable capacity is equal to the maximal net load hour. This can be expressed in vector notation, and the calculation is deterministic given a variable resource capacity, i.e. does not involve any dependence between hour periods.

$$P_{var,t} = X_{var} A_t$$
$$P_{disp,t} = NL_t = \max\{0, L_t - P_{var,t}\}$$
$$X_{disp} = \max_t\{NL_t\} \quad (1)$$

Empirically, load demand in PJM is always significantly positive. For example, even the minimum load hour over the sample (April 4, 2010) saw 43.13 GW of load. So any hour with near-zero variable generation faces positive net load and the overall system would require positive dispatchable capacity. Trivially, the presence of zero-generation hours that occur empirically for solar PV generation (occurring during the night hours) means that solar PV, without storage or demand shifting, has zero power substitutability.

4.3.2 Infinite Storage Capacity Without Time Constraint

As an asymptotic "best case scenario" exercise to consider the maximum possible effect of including energy storage, consider infinite energy storage capacity (MW) with no self-discharge rate (MWh charge can be stored forever with no degradation). Also suppose there is no time asymmetry of thermodynamics, i.e. energy is allowed to "time travel" and sent to prior periods. While obviously impossible, these assumptions can be used to illustrate a bound on the benefits of energy storage to improving substitutability.

The optimal dispatchable capacity is just the arithmetic mean of $v_t = L_t - P_{var,t}$. A simple proof is as follows. Consider time-indexed vector $v: v_t \geq 0$, which is transformed through energy storage to vector $u: u_t \geq 0$, such that energy is conserved and their sums are equal: $\sum_t v_t = \sum_t u_t$. First, having arithmetic mean as the power dispatch at every period is trivially a feasible recombination of individual elements (allowed under the above unrealistic assumptions).

$$u_t = \bar{v}$$
$$\sum_t u_t = \sum_t \bar{v} = T\bar{v} = T\left(\frac{1}{T}\sum_t v_t\right) = \sum_t v_t$$

Suppose for contradiction there is a better solution where the maximal element u_j^* (corresponding to required dispatchable capacity) is less than the mean. By construction the other elements are not maximal $u_t^* \leq u_j^*, \forall t$.

$$u_t^* \leq u_j^* < \bar{v}$$

$$T\bar{v} = \sum_t v_t = \sum_t u_t^* = u_j^* + \sum_{t \neq j} u_t^* < \bar{v} + (T-1)\bar{v} = T\bar{v}$$

The last inequality above is clearly a contradiction, so the arithmetic mean is the minimizer of the vector's maximal element. So the mean is the required dispatchable capacity under the infinite storage, no self-discharge, time travel assumptions.

$$X_{disp} = \frac{1}{T}\sum_t \left(L_t - P_{var,t}\right) \quad (2)$$

Another interpretation of this result is that using simply LCOE (or any metric measuring a normalized cost of average energy generation) to judge electric generation resource substitutability is mathematically equivalent to assuming the presence of infinite storage capacity with the ability of energy to "time travel".

4.3.3 Finite Storage – Perfect Foresight Algorithm

Given the maximum storage capacity and installed intermittent resource capacity as constant parameters, the following linear program solves the optimal schedule of charging. Note that this optimization is not a least-cost optimization, because it ignores economic costs. Rather, this formulation may be illustrative as to the maximum amount of technical substitution of power capacity that could occur under storage. Intuitively, more energy generation during off-peak hours can be stored and used to offset load demand during on-peak hours; however, greater generation volume also requires larger power capacity.

minimize X_{disp}

such that $S_0 = 0$	(Zero initial charge)
$0 \leq P_{stor,t}^- \leq \gamma S_{t-1}$	(Energy available to be discharged)
$0 \leq P_{stor,t}^+ \leq P_{var,t} + X_{disp}$	(Energy available to be stored)
$0 \leq S_t \leq S_{max}$	(Finite energy capacity)
$S_t = \gamma S_{t-1} + P_{stor,t}^+ - P_{stor,t}^-$	(Conservation of energy across time)
$P_{var,t} + X_{disp} - P_{stor,t}^+ + P_{stor,t}^- \geq L_t$	(Resource adequacy to cover load)

Where $P_{stor,t}^- - P_{stor,t}^+$ is the net amount of energy discharged from the storage device in one period. Coefficient γ is the decay rate representing the effect of self-discharge after one period. S_{max} represents the amount of installed energy capacity (MWh) of storage; it is assumed that the installed power capacity (MW) is equal or greater than this value such that there are no ramp rate constraints, i.e. assuming that the storage resources in aggregate can discharge or charge through the entire range of available energy.

The property of the linear program formulation is that the objective function at a solution is guaranteed to be a global extremum. It is generally possible for an LP problem to have multiple solutions leading to the same objective function values; however, in this case the decision variable only has dimension one (MWh of storage capacity) and so the solution is a global minimizer.

When coding the conservation of charge condition, the dynamic relationship between successive time periods is clearly a linear function, and so if $T = 4$ time periods then this can be written in matrix notation:

$$S = \begin{bmatrix} S_0 \\ S_1 \\ S_2 \\ S_3 \end{bmatrix} = \gamma \begin{bmatrix} 0 & 0 & 0 & 0 \\ 1 & 0 & 0 & 0 \\ 0 & 1 & 0 & 0 \\ 0 & 0 & 1 & 0 \end{bmatrix} \begin{bmatrix} S_0 \\ S_1 \\ S_2 \\ S_3 \end{bmatrix} + P^+ - P^- = \gamma MS + P^+ - P^-$$

Generalizing to any size T, this "continuity matrix" M of dimension $T \times T$ is defined as a consisting of a one-off-diagonal identity matrix to capture the decay effect between adjacent time period of storage.

4.3.4 Finite Storage – Myopic Algorithm

The linear programming formulation above has the data vectors accessible across the entire time dimension as decision variables; however, in reality it is impossible to have perfect information about the future, placing a limit on "strategic" charging. Specifically, whereas the solution to the above problem can at any period utilize generation from the dispatchable resource to store for a later period with greater net load, the following greedy or "myopic" algorithm will not make such a choice. Intuitively, the myopic algorithm only chooses to store electric charge when there is excess variable generation above the load requirement for the period. In addition, this myopic algorithm will. This strategy can be written algorithmically with discrete time steps:

Let $S_0 = 0$
For time $t = 1 \ldots T$:

$P^+_{stor,t} = \min\{S_{max} - \gamma S_{t-1},\ \max\{0, P_{var,t} - L_t\}\}$ (Net generation → store)
$P^-_{stor,t} = \min\{\gamma S_{t-1},\ \max\{0,\ L_t - P_{var,t}\}\}$ (Net shortfall → discharge)
$S_t = \gamma S_{t-1} + P^+_{stor,t} - P^-_{stor,t}$
$NL_t = L_t - P_{var,t} - P^-_{stor,t} + P^+_{stor,t}$

Then the required dispatchable capacity can be determined from this sequence of net load values:

$$X_{disp} = \max\{NL_t\}$$

This algorithm runs in O(n) time complexity as it simply requires one pass through the time dimension. Cheng [61] proves that the myopic algorithm (only charge when there is excess renewable generation, and discharge as much as possible to cover net load) is in fact economically optimal under the condition that the dispatchable generation has constant marginal cost and that there is a positive self-discharge rate. Otherwise, intuitively, it may be more cost-effective to store cheaper electricity in this period and then use it to offset more expensive generation in a later period, rather than immediately discharge it in some intermediate period. However, this may not be the optimal algorithm to minimize the necessary backup generator capacity, due to the same intuition of not having optimality guarantee under a rising supply curve structure, i.e. discharging this period during a low net load hour is at the expense of saving and discharging later at the highest net load hour. Later, the optimality gap between these two strategies, which can represent the value of perfect forecast and is conceptually related to the expected value of perfect information, can be empirically determined.

4.3.5 Numerical Results for Power Substitutability

Based on the above theoretical formulations of the amount of capacity substitution, under various assumptions about energy shifting capability, numerical technical substitution curves can be constructed from the data. This section will use the last year of available NREL wind data, 2012, as the year for load and variable renewables (wind and solar) data. The decay factor is assumed to be 98%, i.e. 2% of the energy stored is assumed to spontaneously discharge over a one-hour period. The ranges of parameters chosen to be evaluated are 0 to 1000 GW of installed wind capacity. The effect of storage capacity is modeled as:

- No storage
- Myopic algorithm at 10^1, 10^2, 10^3, 10^4 GWh of storage energy capacity
- Perfect foresight algorithm at 10^1, 10^2, 10^3, 10^4 GWh of storage energy capacity
- Infinite storage without time constraint (equivalent to only considering average capacity factors)

For concrete comparison, the average hourly load in PJM is around 90 GWh, so that once fully charged the high scenario's 10^4 GWh = 10 TWh of energy storage capacity can cover roughly 4.6 days of PJM load on average. In 2017 there is about 7.9 GW of installed nameplate capacity of wind power according to [2], so the high point of 1000 GW = 1 TW of nameplate wind power capacity in the simulations corresponds to about 127 times the current level of deployment.

The closed-form or linear programming formulations (solved by standard interior point method implemented in MATLAB) enable relatively fast numerical computations. Below, each scenario is evaluated at wind capacities ranging from 0 to 1000 GW. The grid resolution for the closed-form computations (no storage, myopic, and infinite storage cases) is 100 MW, i.e. $10^{12}/10^8$ = 10,000 individual points for each scenario. The grid resolution for the foresight case is 10 GW, i.e. $10^{12}/10^{10}$ = 100 individual points for each scenario.

Figure 9: Installed Dispatchable Power Capacity as a Function of Wind Energy Capacity Deployment, with Varying Levels of Storage Using Myopic Strategy

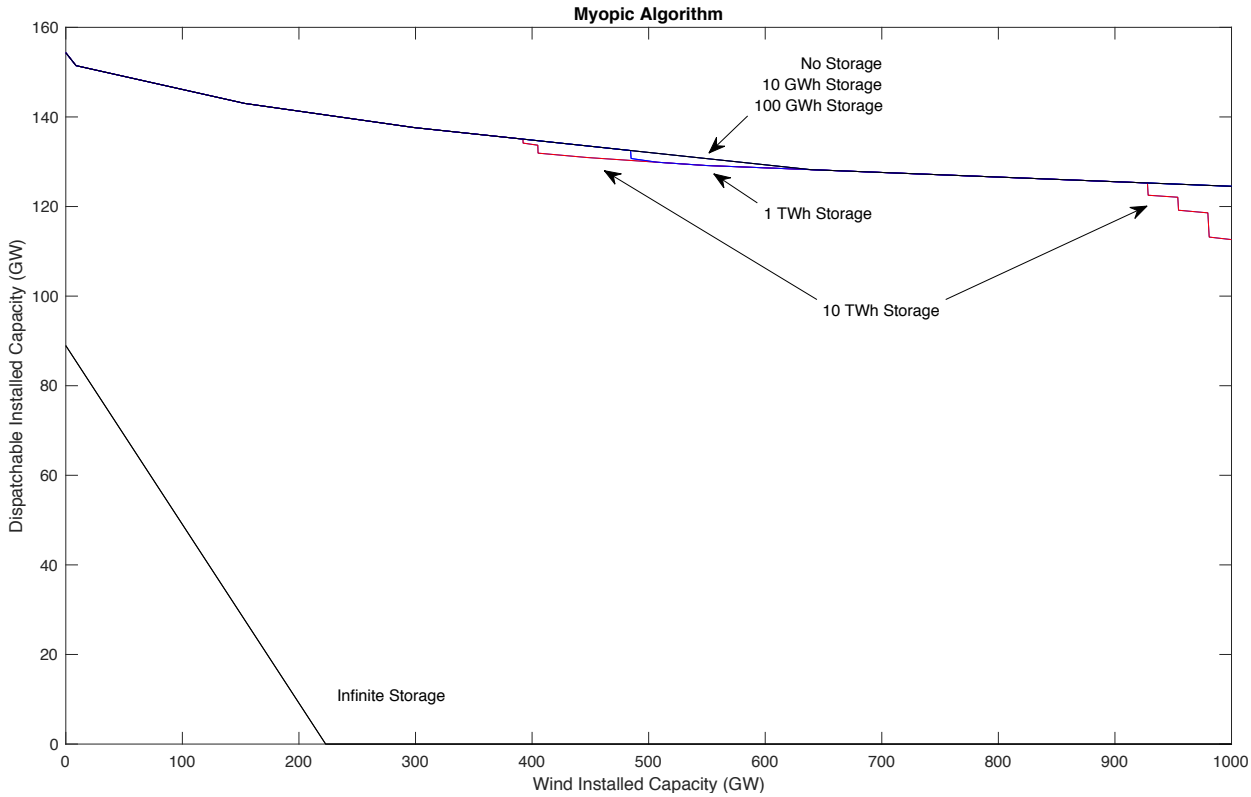

Starting from the no storage case, increasing wind capacity leads to a monotonically decreasing amount of dispatchable (e.g. gas) power capacity. However, the overall shape is convex, i.e. greater amounts of wind leads to diminishing substitutability, which can be viewed as the "saturation" of a particular type of renewables.

Using the above implementation of a myopic or greedy algorithm, the addition of energy storage does not noticeably decrease the required amount of dispatchable capacity. Intuitively, even though the high-wind scenarios (towards the right of each plot) would produce significant excess generation, the myopic algorithm would have expended it all at the wrong times, rather than decreasing the peak hour net loads.

The infinite storage capacity allowing for "time travel" of energy between periods shows a simple piecewise linear decrease in the required power capacity until zero. The vertical gap between this naïve curve and any of the other substitution curves illustrates the inadequacy of relying on only energy generation substitution for evaluating comparative energy systems.

Figure 10: Installed Dispatchable Power Capacity as a Function of Wind Energy Capacity Deployment, with Varying Levels of Storage Using Perfect Foresight Strategy

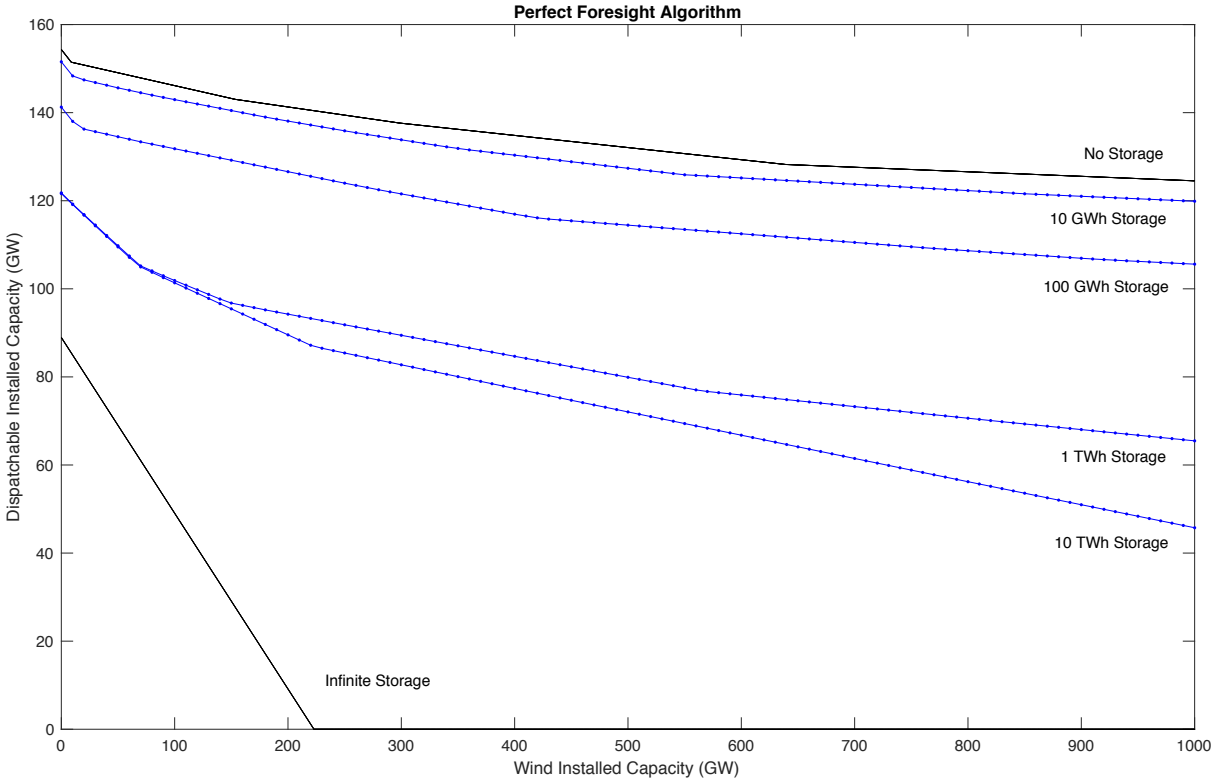

In comparison, the perfect foresight algorithm leads to a much more noticeable decrease of required dispatch capacity, with the magnitude of capacity substitution increasing with larger amounts of storage capacity available. At each given level of wind capacity, the vertical difference between the achievable substitution between using the myopic versus perfect foresight algorithm represents an optimality gap from imperfect information. This implies that incorporating load and renewables forecasts to strategically charge or discharge storage units has high value.

Despite this difference in results between the two charging algorithm formulations, the technical substitution achievable under perfect future information has an overall smaller slope than the infinite storage case, and also exhibits the convexity or saturation of high levels of renewables seen under the no storage case.

The underlying principle of lock-in related to the time structure of costs. The first two analytical sections directly account for costs and examine conditions and properties of economic costs that lead to lock-in. However, these analyses assume a perfectly substitutable resource, i.e. an energy resource that is also dispatchable. The reality of variable renewable resources is highly intermittent. In this context, this last analytical section on capacity substitutability serves as a best-case-scenario bound for how much renewables can feasibly replace

The implication of this bounding exercise for the analysis of carbon lock-in conditions is that the extent of carbon lock-in is likely limited, because even under scenarios with high

amounts of renewables as well as energy storage there is still a resource adequacy need for dispatchable resources (even if they might end up with much smaller dispatched capacity values). Even under conditions where the average generation analysis would suggest the existence of lock-in, the limited power substitutability between variable renewable resources (e.g. wind) and dispatchable resources (e.g. natural gas combined cycle) restrict the amount of lock-in that can actually occur. However, the inclusion of energy storage resources (which can be viewed as mathematically related to shifting demand) would improve the power substitutability of variable renewable sources. This may suggest that carbon lock-in may present an issue in the future, as energy storage resources continue to improve in cost and performance, if externalities continue to not be fully accounted.

5. Empirical Assessment of Optimization Path Dependence

5.1 Optimization Assumptions

Given existing resource capacities, the problem is to find the least-cost mix of new capacity expansion and expected generation dispatch to meet load, allowing capacity factors to adjust endogenously. The objective is to minimize system generation costs, subject to the constraints that generation satisfies load demand in all hours and that thermal generators meet various operational requirements. The scope of generation types will encompass conventional thermal (nuclear, coal, natural gas combined cycle, natural gas combustion turbine), hydropower, variable renewables (wind turbine, solar photovoltaic), and energy storage.

Various modeling assumptions are made to simplify the formulation for better interpretability of results, including:

- To roughly reflect actual market conditions, only gas combined cycle and variable renewables are assumed to be able to have new build, i.e. have capacity expansion decision variables. Energy storage will be included as a robustness check, but will be assumed to exist exogenously without any costs as a bounding exercise.
- Variable renewable generation will be modelled based on capacity factor values (from 0 to 100% of nameplate capacity) that are exogenous random variables. The solar PV generation data series are constructed using assumptions more consistent with utility-scale solar, as opposed to distributed solar such as residential or commercial rooftop installations. Each type of electricity resource will each be modelled as a single system-wide unit, with continuous levels of output. In reality, different individual generators can have very heterogeneous operating and cost characteristics. Rather than a linear continuous variable, many generators also have significant nonlinearities in the operating range, e.g. start-up costs, minimum load.
- For simplicity, the model will use a “copper plate” assumption, i.e. that the transmission system always has sufficient capacity and incurs no resistive line losses, which is often used for intra-regional modelling in capacity planning studies as described in Frew et al. The lack of transmission modelling and AC power flow is a limitation that distinguishes this model from a more real-time operational model such as optimal power flow (OPF).
- Electric load demand will be assumed to be an exogenous variable that is perfectly inelastic. It is important to note that on wholesale markets, demand response (where load demand is dynamically reduced to follow market signals) already contributes to PJM system capacity and leads to significant cost savings. On the level of electric distribution systems, dynamic pricing systems like time-of-use (TOU) utility tariff structures have the possibility to lead to partially elastic electric demand that respond to system generation costs, i.e. demand becomes endogenous.

5.2 Linear Program Formulation: Capacity Expansion

Variable Sets

i	Resource type: coal, gas (CT and CC), wind, solar, nuclear, hydro (Size 7)
t	Time hour of the year (Size 8760 * N years)

Exogenous parameters: economic costs

$k(i)$	Capital cost for power capacity, in $ / MW
$f(i)$	Annual fixed operating and maintenance cost, in $ / MW
$v(i)$	Variable fuel costs for energy generation, in $ / MWh
$s(i)$	Variable externality costs for energy generation, in $ / MWh

Exogenous parameters: physical parameters

$X_{old}(i)$	Existing power nameplate capacity at start of period, in MW
$r(i)$	Ramp rate, in MWh output that can be adjusted up or down in 1 hour per MW capacity (%)
$l(t)$	Load demand (RTO-level metered load) in given hour, in MWh
$a(i,t)$	Physically available capacity value of resource, in dimensionless % (Assumed to be always 1 for resources that are not wind or solar.)

Decision variables

$X_{new}(i)$	New power capacity to be constructed, in MW
$P(i,t)$	Dispatch of each resource type for each hour, in MWh

minimize	$C_{cap} + C_{fin} + C_{ext}$	(Objective function)
subject to	$\forall i: X_i = X_{old,i} + X_{new,i}$	
	$C_{cap} = \sum_i A_{r,n_i} k_i X_{new,i}$	(Capital costs)
	$C_{fin} = \sum_i \left(f_i X_i + \frac{1}{N} v_i \sum_t P_{i,t} \right)$	(Operating monetary costs)
	$C_{ext} = \sum_i \left(\frac{1}{N} s_i \sum_t P_{i,t} \right)$	(Operating externality costs)
	$\forall i,t: \quad P_{i,t} \le X_i a_{i,t}$	(Generation resource adequacy)
	$\forall i,t: \quad -r_i X_i \le P_{i,t} - P_{i,t-1} \le r_i X_i$	(Ramping constraint)
	$Q_0 = 0$	(Zero initial storage charge)
	$0 \le P^-_{stor,t} \le \gamma Q_{t-1}$	(Energy available to be discharged)
	$0 \le P^+_{stor,t} \le \sum_{i=1}^{n} P_{i,t}$	(Energy available to be stored)
	$0 \le Q_t \le Q_{max}$	(Finite, positive energy capacity)
	$Q_t = \gamma Q_{t-1} + P^+_{stor,t} - P^-_{stor,t}$	(Conservation of energy across time)
	$\forall t: \quad \sum_{i=1}^{n} P_{i,t} - P^+_{stor,t} + P^-_{stor,t} \ge L_t$	(Hourly load balance)

The annuity factor $A_{r,n} = \frac{r}{1-\left(\frac{1}{1+r}\right)^n} K$ relates a capital payment today to a series, with equivalent present value, of future annuity payments over the n_i periods in the resource type's lifetime, and can be represented as a debt and equity repayment or amortization schedule with a closed-form analytical value. The financial discount rate is r_f, which can be interpreted as a weighted cost of capital (7% used). The social discount rate is r_s, which can in general be different from financial intertemporal tradeoff (3% used). In practice these get mixed, which confuses the conceptual purpose of using discount rates to represent intertemporal tradeoffs of value. For example, Noel et al uses 3% for all costs. The EPA Clean Power Plan repeal proposal's regulatory impact analysis uses either all 3% or all 7%. It is possible to consider inter-annual variability by interpreting the variable costs (which depend on the physical stochastic variables) as the expectation over the N different yearly realizations $E\left[P_{annual,i}\right] = \frac{\sum_t P_{i,t}}{N}$. Another interpretation of this possible approach is a Monte Carlo simulation, where the stochastic variables of load and renewables retain their statistical correlation structures.

Algorithmically, the linear structure of the LP problem, in terms of objective function and constraints, guarantees global optimality of the solution. The solutions are obtained using MATLAB with standard optimization solvers; the model is also verified to obtain the same results using the General Algebraic Modeling System (GAMS).

5.3 Path Dependence Methodology

Starting from the assumed set of existing resources, find the extent of path dependence or carbon lock-in by comparing the optimal solutions between two different trajectories of enforced carbon price:

- "Always 50": Always full, "true" carbon price reflecting the social cost of carbon. The optimal solution in this trajectory represents the global optimum from today's perspective.
- "First 0, Then 50": First no carbon price, resulting in a set of optimal new capacity builds. Starting from this new set of existing plus new capacities, then apply the full, "true" carbon price. The optimal solution in this trajectory represents the local optimal from the perspective after a carbon pricing delay.

The difference between the optimal solutions of these two different trajectories therefore exactly represents a measure of the regret function, as discusses in the literature review. A relatively larger deviation that exists between these two cases signifies a larger degree of carbon lock-in exists.

Note that first this analysis the second period of "Then 50" is assumed to effectively start immediately after the initial first period investments are committed; in reality, during the interim period some of the committed fossil fuel resources may retire due to lifetime depreciation, and renewables capital costs may have decreased. These effects in the interim time interval are not captured by this method, but can reduce the effect of lock-in. Therefore, the following analysis could be interpreted as a bounding case, where such additional circumstances can further reduce the lock-in magnitude.

5.4 Cost Parameters

Cost input parameters are mainly taken from the Energy Information Administration's 2017 Annual Energy Outlook, using the ReliabilityFirst – East (RFCE)[1] values for capital costs to account for geographical drivers for costs in the PJM region [97]. Financial costs (all economic costs except for pollution externalities) are assumed to be time-discounted according to $A_{7\%,20} = 9.44\%$ and $A_{7\%,30} = 8.06\%$. Social costs (just pollution externalities) are assumed to have a lower intertemporal tradeoff based on intergenerational equity, and so externality operating costs are adjusted by $A_{3\%,20} = 6.72\%$, i.e. increased by a scalar $\frac{A_{7\%,20}}{A_{3\%,20}} = 1.40$. Wind and solar are assumed to have a 20% reduction in fixed costs.

Carbon dioxide emissions are based from EIA values [98]. Natural gas fugitive emissions are accounted for by assuming a 1% leakage rate and an 86-times global warming potential of methane compared to carbon dioxide,[2] based on the IPCC Fifth Assessment Report [3]. Fugitive emissions are converted to an energy content basis via the energy gravimetric density of liquefied natural gas (LNG) and assuming mass conservation [99]. Nuclear fuel costs are taken from Haratyk's estimate of 2015 mid-Atlantic nuclear plants [100].

Table 7: Natural Gas and Coal Variable Cost Assumptions by Chemical Energy Content

Fuel Type	Natural Gas	Coal
Fuel Price ($ / MMBtu)	4	2
Combustion Emission Rate (kg CO_2 / MMBtu)	53.07	93.35
Natural Gas Energy Density (kg CH_4 / MMBtu)	$(1 / 53.4)10^3 = 18.73$	NA
Natural Gas Fugitive Emission Rate	1%	
Global Warming Potential Multiplier of CH_4 vs. CO_2	86	

Table 8: Cost Assumptions by Resource Types

Resource Type	Units	Gas CC	Onshore Wind	Solar PV	Gas CT	Coal	Nuclear	Hydro
Overnight Capital	$/kW	1283	2271	2524	Assume no new buildout			
Assumed Lifetime	years	20	20	30				
Capital Annuity	$/kW/year	121.11	171.51	162.70				
Fixed O&M	$/kW/year	9.94	46.71	21.66	6.76	70	100	15
Fixed Cost	$/kW/year	131	209	180	6.76	70	166	15
Variable O&M	$/MWh	1.99	0	0	10.63	7.06	2.29	2.66
Heat Rate	MMBtu/MWh	6.3	0	0	9.8	9.75	0	0
Variable Fin. Cost	$/MWh	27	0	0	50	27	0	0
Variable Carbon Cost	$/MWh	21.79	0	0	33.91	43.58	0	0
Total Variable Cost	$/MWh	58	0	0	97	88	2.3	2.7

[1] ReliabilityFirst is a Regional Entity approved by the Federal Energy Regulatory Commission to oversee bulk power system reliability in the Eastern Interconnection, and is a geographical superset of the PJM region.

[2] The global warming potential of 86 for methane is based on a 20-year lifetime, which is consistent for the power system study period, and includes climate-carbon feedback effects.

5.5 Optimization Numerical Results

5.5.1 Starting from Zero Installed Capacity

Results here use simple equal-weighted means of wind and solar.

Table 9: "Long term, greenfield" – Starting from 0 existing capacity

Carbon Price ($ / ton)	Capacity (GW)			Energy Share (%)		
	Always 0	First 0, Then 50	Always 50	Always 0	First 0, Then 50	Always 50
CT	57.63	**51.87**	**52.01**	3.92	**1.77**	**2.38**
CC	98.53	**98.53**	**81.36**	96.08	**72.63**	**56.71**
Wind	0	**57.74**	**79.02**	0	**25.60**	**35.00**
Solar	0	**0**	**22.56**	0	**0**	**5.90**

The results in the above table imply that due to the economic path dependency effect caused by sunk costs alone, the prior period buildout of gas capacity "locks out" about 9.4% of gas generation share (corresponding to 21.3 GW of capacity) and all 5.9% of solar generation share (corresponding to 22.56 GW of capacity) from being economically included in the optimal solution. In other words, the presence of the extra 17 GW of pre-existing combined-cycle gas capacity was extraneous and led to the path dependent effect.

Parametrizing on the carbon price level, the above two-trajectory calculation framework can be applied to find the extent of carbon lock-in effect over a wider range of beliefs on the social cost of carbon. The traces are plotted below. The patterns for locked-out capacity levels are linear transforms of these plots, since solar and wind production is determined for a given level of capacity, i.e. assuming no renewable curtailments. Further, each lock-out curve can be calculated for different assumptions about renewable energy cost declines; the following plots show 0%, 20% (reference case), and 40% cost declines. This allows the timeframe of analysis to be abstracted.

Figure 11: Optimal Renewable Shares, Comparing First 0 Then X vs. Always X Carbon Prices

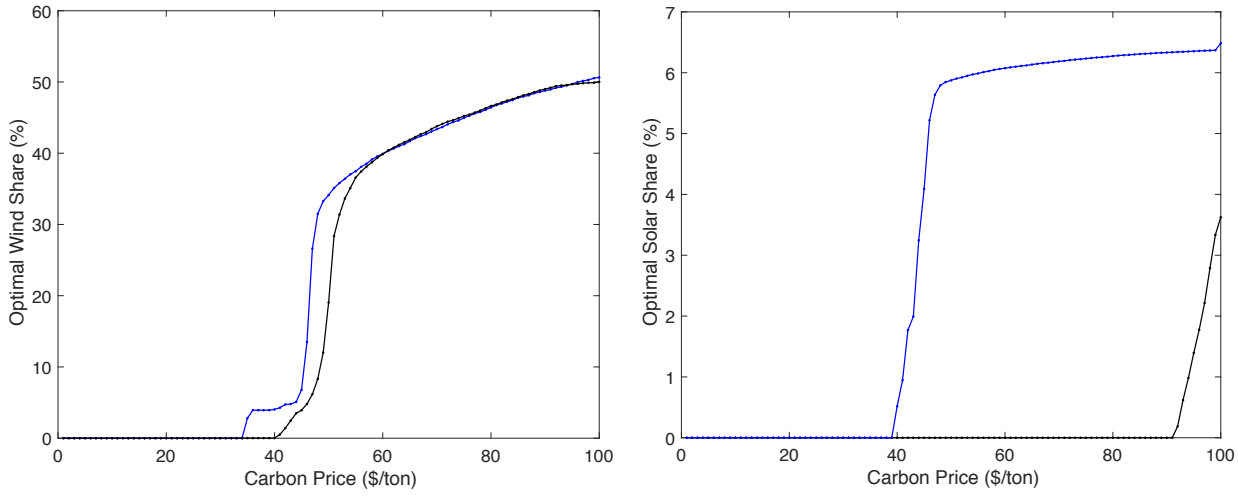

Figure 12: Regret or Path Dependence Lock-Out Magnitudes for Solar and Wind Power

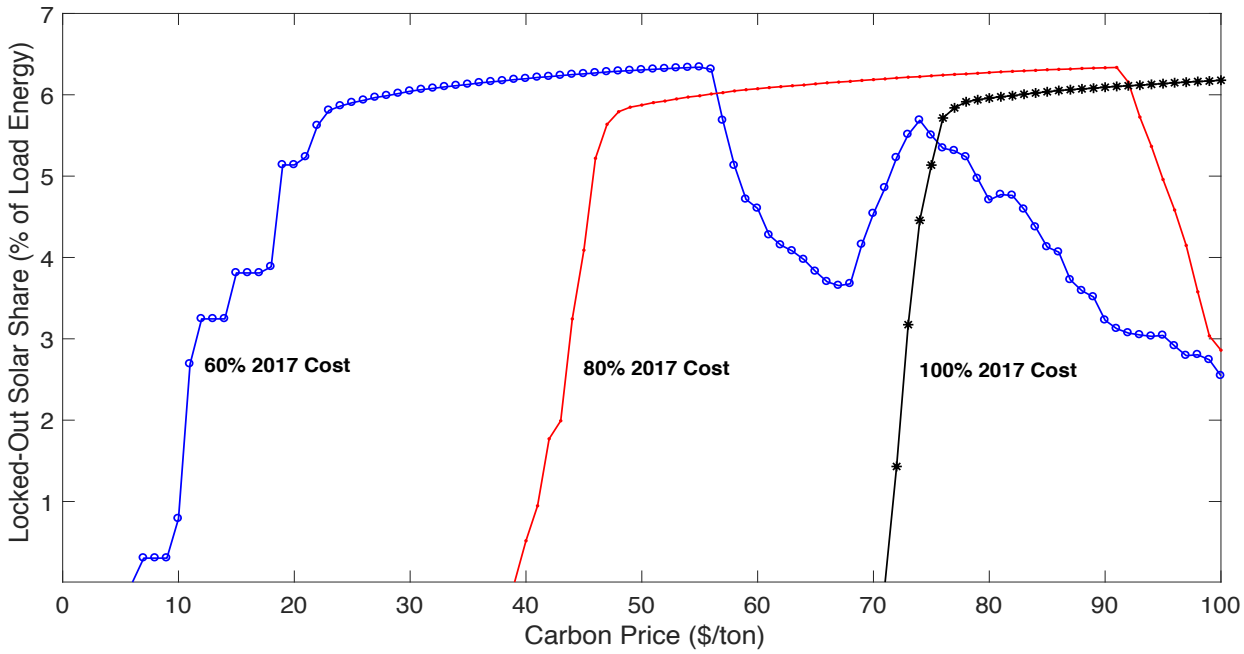

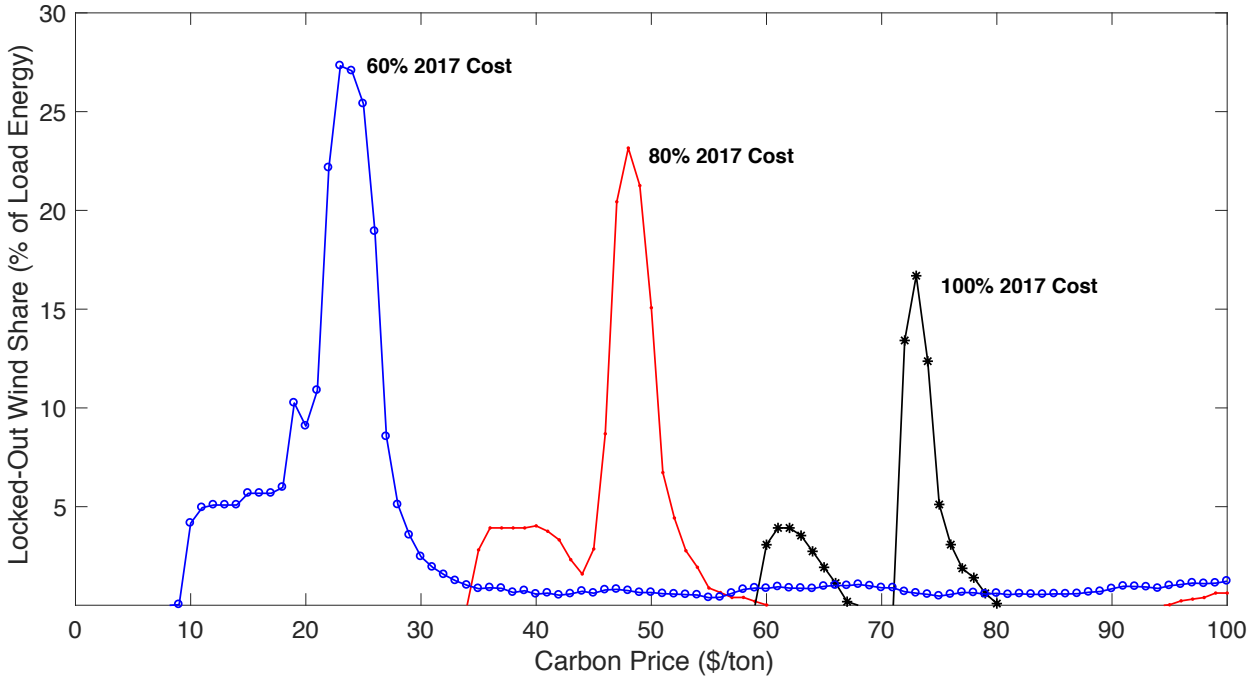

For both wind and solar, the first-0-then-50 curve roughly appears to be a delayed version of the always-50 curve, in terms of the carbon price domain. In simple terms, if the "true" carbon price is too low, then delaying its implementation does not matter because even in its presence the renewable technology does not appear in the optimal mix. Conversely, if the "true" carbon price is very high, then its implementation even if delayed still leads to high levels of renewables and thus decreased lock-in effect. This results in a peak pattern shown empirically in the above

plots, with the width of carbon prices compatible with lock-in for wind being much narrower than that for solar.

For reference, recall the lock-in range for wind calculated in the earlier section is about $31 to $59, which corresponds roughly to the area of active lock-in shown below for the 20% cost reduction case (red line). While the earlier analytical framework enabled calculating the range of lock-in prices, using numerical optimization allows for the direct consideration of dynamic load and intermittent renewable generation. The optimization framework further enables calculating the magnitude of the lock-in effect at different parameter values, as a function of these various complicating factors.

Together these regret or lock-out curves explicitly demonstrate the properties of the carbon lock-in mechanism. When renewable energy costs decrease, the optimal share from the renewable resource increases, which in turn makes it “easier” for lock-in to occur in that the carbon lock-in range of prices tends to shift leftward on the plots. This means that as renewable energy costs decline, it would require one to believe progressively in lower and lower “true” social costs of carbon for tbe regret of lock-in to materialize.

Additionally, the lock-out curves for wind power shows not just a leftward shift of the lock-in range, but that the mangitude of the regret function in terms of the peak actually increases as the renewables installation cost declines.

5.5.2 Starting from Existing Installed Capacity

Results here use the mean-variance optimized wind series, and equal-weighted solar.

Existing resource capacity values as of June 30, 2017 can be found from PJM's independent market monitor report [101].[3] From this existing fleet, exogenous assumptions are made about retirements of coal and nuclear capacity that have been announced or are likely to occur based on market economics. The rationale for this approach, rather than estimating economic retirements endogenously in the model, is that there is significant heterogeneity between the cost and performance profiles of individual generators. Haratyk calculates based on simulation that the PJM region's average profitability of nuclear power plants is slightly positive over 2017 to 2019, but individual plants in the region range in profitability roughly from negative $8 / MWh to positive $14 / MWh. The simplified optimization model treating each resource type as a homogenous resource is unable to capture this type of supplier heterogeneity. So the following calculations assume retirement of nuclear plants identified by Haratyk and geographically in PJM to be unprofitable,[4] accounting for about 8.5 GW of nameplate capacity.

Table 10: Start with existing – Assume some exogenous retirements of both coal and nuclear

	Capacity (GW)				**Energy Share (%)**			
CO_2 Price ($ / ton)	Existing	Always 0	FZTF	Always 50	Always 0	FZTF	Always 50	**Δ**
CC	41.05	48.12	48.12	46.68	29.36	33.16	32.47	**-0.69**
Wind	7.92	7.92	56.61	57.63	3.36	24.01	24.44	**+0.43**
Solar	0.88	0.88	5.07	5.01	0.22	1.28	1.26	**-0.02**
Coal	47.62	47.62	31.14	32.57	29.10	3.56	3.86	**+0.30**
Nuclear	25.27	25.27	25.27	25.27	27.07	27.07	27.01	**-0.06**
Hydro	9.91	9.91	9.91	9.91	10.62	10.53	10.51	**-0.02**
CT	25.25	25.25	25.25	25.25	0.27	0.40	0.39	**-0.10**

Here the 0 carbon price initial period sees 7 GW capacity expansion as optimal, which is significantly smaller in magnitude than in the starting from zero case. Contrary to the results from the starting from zero setting, the above table implies there is less than a 0.5% effect in terms of locked-out renewable generation share. Specifically, wind output share is permanently locked-out by only 0.43%, while the optimal level of solar generation does not appear to be disrupted by the new gas build. In effect, the presence of pre-existing capacities of other resources reduces the amount of optimal gas buildout, as well as prevent the lock-in effect from occurring.

[3] Table 12-12 shows capacity in PJM by resource type in terms of nameplate capacity, so the values shown differ "from capacity market installed capacity because it includes energy-only units, excludes all external units, and uses nameplate values for solar and wind resources." Further, all "steam" generator capacity is assumed to use coal as fuel source, while in reality steam turbines can use other fuel sources like natural gas.

[4] Nuclear plants with negative net profits after including any zero emission credit (ZEC) subsidies in Haratyk's Figure 2, with plants in PJM being Byron, Three Mile Island, Oyster Creek, Quad Cities, Hope Creek, Beaver Valley [100].

The reason that the pre-existence of resource capacities essentially eliminates the lock-out effect is because the optimal amount of natural gas CC capacity in the "always 0" scenario, here 48.12 GW is significantly lower than that in the "always 0" scenario with no other dispatchable resources, namely 98.53 GW. The fact that the "always 50" ideal scenario sees only a slightly lower level of natural gas CC buildout, with the optimal capacity level at 46.68 GW, means the amount of initial buildout in the "first 0" period does not have a large enough magnitude to trigger lock-in.

This result relies on the initial period investments being endogenously driven by optimization. It is also instructive to examine the path dependence effect of additional natural gas generation buildout, at levels beyond what is deemed optimal by the assumed model parameters.[5] The optimal shares for nuclear and hydro do not see significant changes more than 0.1% among these cases, intuitively because the inclusion of carbon emission externalities does not affect their marginal cost structure (and the model assumes no new investments in these types).

Table 11: Optimal Capacity Expansion and Generation Shares for Coal and Renewables, Under Increasing Levels of Initial Gas Combined-Cycle Capacity

	Starting CC (GW)	**48**	**55**	**60**	**70**	**90**	**100**
Δ Capacity (GW)	Coal	–16.48	**–23.16**	–23.39	–35.58	–47.62	–47.62
	Solar	4.19	3.95	**0**	0	0	0
	Wind	48.69	47.80	47.23	47.23	**19.64**	0
Energy Share (%)	Coal	3.56	**2.30**	1.84	0.74	0	0
	Solar	1.28	1.22	**0.22**	0.22	0.22	0.22
	Wind	24.01	23.63	23.39	23.39	**11.70**	3.36

The above table marks the first entry in each row where the optimal energy share differs by more than 1% from the 48 GW gas case, roughly revealing at what point each of coal, solar, and wind is affected by the increasing gas buildout.

The overall pattern is that further natural gas combined cycle expansions immediately substitute for both the capacity and energy value of the existing coal capacity, rather than significantly displacing the usage of renewables. The displacement of coal starts immediately, even at 48 GW. The effect of solar also starts soon at around 55 GW of gas CC, or around 14 GW of new combined cycle capacity. However, the magnitude of lock-out against solar is limited because it is bounded by the globally optimal solar share of about 1.3%. The increasing initial gas capacity only starts to affect wind capacity around 90 GW of gas CC, or around 49 GW of new combined cycle capacity, which is after coal usage is completely eliminated with all existing coal capacity retired. These results suggest that as long as there is still pre-existing coal (or some other) resource, then additional gas capacity buildout will compete away with that resource rather than take away market share of wind.

[5] The fact that actual market conditions may exceed the model-identified optimal natural gas power expansion does not necessarily mean the market outcomes are suboptimal. Among other factors, the simplified model does not capture supplier heterogeneity within gas CC.

Table 12: Effect of Exogenous Inclusion of Energy Storage Capacity on Lock-In Effect

	Storage Capacity	**10 GWh**			**262 GWh**	
	Carbon Price ($/ton)	**0**	**FZTF**	**50**	**0**	**50**
Δ Capacity (GW)	Gas CC	4.27	0	0	0	0
	Wind	0	50.64	53.92	0	62.58
	Solar	0	0	0	0	0
Energy Share (%)	Gas CC	28.44	32.58	30.16	27.03	28.68
	Wind	3.36	24.83	26.22	3.36	29.77
	Solar	0.22	0.22	0.22	0.22	0.22

With 10 GWh of storage capacity, which roughly corresponds to being able to serve 10% of average hourly load, the model implies 26.22 – 24.83 = 1.39% of wind generation share lock-out. This effect is larger in magnitude than the 0.4% from the earlier scenario without storage. However, the inclusion of this storage capacity results in the removal of solar from even the always-50 trajectory – this elimination appears to outweigh the slightly larger wind lock-out effect. Furthermore, while higher levels of storage enable higher levels of wind to be optimal (262 GWh is the optimal level of storage if it has zero cost, given assumed cost parameters), this higher storage capacity also precludes new gas capacity from being included as optimal. Thus the high-storage case cannot lead to carbon lock-in by the given definition.

Table 13: Effect of nuclear retirements.
Start with existing – Assume exogenous retirements of only coal, but not nuclear

Carbon Price ($ / ton)	**Capacity (GW)** Existing	Always 0	Always 50	**Energy Share (%)** Always 0	Always 50
CC	**41.05**	**41.05**	41.05	23.24	25.52
Wind	**7.92**	**7.92**	54.56	3.36	23.13
Solar	**0.88**	**0.88**	4.82	0.22	1.22
Coal	**47.62**	**46.23**	30.29	26.16	3.86
Nuclear	**33.73**	**33.73**	33.73	36.14	36.12
Hydro	**9.91**	**9.91**	9.91	10.62	10.23
CT	**25.25**	**25.25**	25.25	0.27	0.39

If no nuclear capacity is retired, then the optimal solution sees no new natural gas combined cycle capacity expansion. In fact, the only capacity change from the status quo scenario is the endogenous retirement of 26.63 GW of coal. Therefore, by definition the lack of new gas capacity buildout in the optimal solution means there cannot be any carbon lock-in effect. If nuclear capacity remains, even without a carbon price, then the privately optimal mix will contain slightly lower levels of renewables compared to the earlier always-50 case (with some exogenous nuclear retirements). Still, if all nuclear capacity remains, the overall carbon emissions appear to be lower than in the earlier case with exogenous retirements under both the "always 50" and "first 0 then 50" scenarios which have higher optimal shares of coal and natural gas generation, compared to nuclear – a zero carbon emission source.

5.5.3 Discussion

Extensive carbon lock-in has been demonstrated theoretically and empirically, especially in the "greenfield" or "long-term" scenario of starting from zero initial resources. However, the currently existing fleet of resources could be considered an exogenous source of path-dependency as well. The numerical results show that existing resources reduce the possible market share that can be optimally attained by renewables. This effect specifically arises from nuclear and hydropower that have low marginal costs not affected by a carbon price (versus coal which endogenously retires and decreases in capacity value under the model). Empirically, gas buildout does not appear to create a significant lock-in effect because it first displaces coal usage, rather than new renewables deployment. Moreover, the no-coal case still has high levels of gas capacity needed for capacity value, as analyzed in the capacity substitution section where variable renewables are shown to have limited capacity substitutability.

However, the earlier analysis and simulation results show that continued renewable cost declines as well as the evolution of various other parameters can both increase the magnitude of the carbon lock-in effect as well as well as decrease the bound of how high one must believe the true social cost of carbon in order for lock-in to exist (or equivalently, widen the lock-in price range). Preliminary results show that the presence of energy storage resources also appears to exacerbate the lock-out effect against wind capacity, because as a complementary resource energy storage increases the optimal amount of wind generation in the "always 50" scenario.

In addition, the lock-out of solar is more pressing since the effect begins earlier, and exists for current planned levels of natural gas capacity expansion. The model only explicitly considers the generation profile and cost structure of utility-scale solar, which may not directly apply to distributed solar. While the magnitude appears small, the reduced installment of solar in the PJM region – even if minor in scale – may amplify in effect by preventing future cost reductions driven by economic learning-by-doing. The same feedback mechanism applies to any amount of lock-out against wind resources, even if the magnitude may appear small.

The demonstrated presence of carbon lock-in combined with the complex and uncertain factors that can exacerbate it contrast strongly with the simplicity of the solution that by construction can prevent lock-in: carbon pricing. The policy implication of these analyses is that delays in implementing a carbon price reflecting the full social cost of carbon will not only continue the existence of the negative externality as a first-order effect, but the path dependence in fossil fuel power capacity buildout has the potential to permanently alter (within the operational lifetimes) the optimal deployment of clean energy resources. This implies that the path dependence effect, in addition to the negative externality itself, serves as another justification for timely implementation of carbon pricing. At the same time, the absence of a very strong second-order lock-in effect (which if it existed would point to urgency in pricing the externality) should not be taken to diminish the important of the first-order climate damages from the externality. Even without any lock-in effects, carbon pricing is still the cost effective, economically efficient policy measure to address greenhouse gas externalities.

Another policy implication is that nuclear retirements appear to worsen the lock-in effect. If nuclear is allowed to retire, then the privately optimal gas buildout would likely cause

additional carbon lock-in, creating some degree of path dependence. Moreover, while coal endogenously retires (mostly due to gas without any carbon pricing), even when assuming no flexibility for nuclear, the nuclear capacity still stays within the optimal solution under the assumed model. This suggests that policy options to properly compensate nuclear generators for their low-emission attribute, such as a consistent market-wide carbon price, would be beneficial over more generic support of all baseload-type resources.

As noted, the numerical modeling approach utilizes many simplifying assumptions, so the above results should be interpreted in this context. Many factors that are not explicitly considered by the model would logically decrease the optimal share of renewables, and would in fact strengthen the result of carbon lock-in being negligible. For example, costs for cycling costs (from mechanical wear due to repeated ramping) and ancillary services of various types are not included in the objective function, and realistically may increase in a high-renewables scenario. On the other hand, outage rates (e.g. for planned maintenance) are not modeled for conventional power plants, which implicitly have an available capacity factor of one. Incorporating more realistic capacity availability would increase the effective capital costs for these resources.

Other factors not being considered here also relate to the dynamic growth of the optimal renewables share over time, as opposed to just an optimal solution in a static sense. In particular, renewable energy cost declines over time, which are not explicitly or dynamically modeled here, can mean that a static optimal solution of low renewables today will be quickly followed by optimal high renewables in a subsequent period. The historical trend of solar and wind cost decline curves, combined with analyst projections based on economies of scale and learning effects, suggest that relatively steep cost decline curves are likely to continue for solar and wind. This means that the interim interval, mentioned earlier in the numerical methodology section, may in fact result in substantial cost declines that eliminate the lock-in effect (which would be estimated to occur if the cost structures had remained static). The similar directionality would result from increasing natural gas prices, which could feasibly come about from increased demand from the power sector (not modeled endogenously with a general equilibrium approach here) or liquefied natural gas (LNG) exports. The most likely directions of these factors suggest that the results about negligible lock-in effect are robust, i.e. that carbon lock-in can be mostly escaped in PJM. However, there may still be interaction effects that warrant further study with more detail, taking these factors into consideration.

Conversely, there are also factors not considered that can deepen the lock-in effect. Most prominently, the early literature on economic path dependence focuses on increasing returns such as that experienced with network externalities. Both Unruh and Erickson et al. identify energy infrastructure networks as possible sources of lock-in, where continued development of the required upstream supply chain via capital-intensive pipeline networks can entrench incumbent technology usage, along with organizational inertia. While social and political inertia may be more challenging to model without using subjective parameters, it may be valuable for future studies to explicitly explore the gas-electricity interface and the associated possibility for lock-in due to these interaction effects. In particular, the framework proffered in this thesis, which relies mathematically on a regret function applied to readily computable cost structures, might be applicable to an integrated gas-electricity system model.

6. Conclusion

The prior literature dealing specifically with carbon lock-in is either overly simplistic by ignoring the value of capacity as in [5], or is "too" detailed as in the national-level capacity expansion modeling in [7] such that it is not as amenable to deep interpretability. Seeking to contribute novel understanding to this issue, this thesis analyzes simplified mathematical settings to highlight the most salient features of the capacity expansion optimization problem. In effect, there are three crucial distinctions between the LCOE analysis in [5] and the "fully-detailed" numerical modeling in [7]. This thesis analyzes each of these three characteristics separately based on first principles, in order to assess the impact on overall path dependence.

First, assessing a regret function on the optimization outcomes under two counterfactual carbon policy scenarios requires that this carbon policy has additionality; mathematically this translates to a lower bound condition not considered by the original LCOE comparison (which only addresses the upper bound). The novel algebraic expression for the carbon lock-in price range, resulting from the first analytical section of this thesis, serves to simultaneously account for both lower and upper bounds. In short, whether carbon lock-in exists is a function of one's belief on the actual social cost of carbon, and this believed level must fall within the lock-in range (in turn a function of economic cost parameters) for undesirable path dependence to occur.

Second, comparing levelized or energy-normalized costs does not account for the fact that electricity is valued very differently at different times. This can be interpreted as a direct consequence of intermittency on the part of load demand: the variability of electric load is readily seen in the shape of a load duration curve. A calculus-based derivation, based on a local optimality argument, results in a novel closed-form solution for the capacity expansion problem with perfectly dispatchable resources. Then in this framework, the derivation demonstrates mathematically that a lock-in effect only exists if the committed sunk resources exceed the counterfactual optimal level. In other words, if the level of existing resources is not high enough, then the next period optimal solution will still converge to that in the original case. This rigorously establishes the notion that the initial period "over-building" must be large enough for lock-in to have a significant magnitude.

Third, the analysis thus far still assumes the energy resources are substitutable after being normalized by energy; in reality renewable energy sources are intermittent. Therefore, technical substitution curves are traced under different assumptions about the availability and sophistication of energy storage technology and operations. The limited ability to substitute away the power capacity of dispatchable sources means that the lock-in effect against a renewable resource must necessarily be smaller (although it can still be positive) than that of a perfectly dispatchable resource under the first two analytical building blocks above, holding all other cost parameters equal.

Finally, numerical modeling based on LP optimization shows that carbon lock-in can exist under realistic parameters in the PJM region. However, the magnitude of lock-in greatly decreases with the addition of PJM's existing resources, including nuclear, hydropower, and coal. These results are consistent with the three analytical building blocks, and are discussed along with policy implications and model limitations.

7. References

[1] Rogers, Howard. 2011. "Shale gas—the unfolding story." *Oxford Review of Economic Policy* 27, no. 1 (March): 117-143.

[2] Dumoulin-Smith, Julien, Jerimiah Booream, Mark Piorkowski. 2017. "US Electric Utilities & IPPs: Where's All The Gas Build Coming From?" UBS Global Research. February 3, 2017. https://neo.ubs.com/shared/d1QlBB5rMNXCdOf/.

[3] Myhre, Gunnar, Drew Shindell, François-Marie Bréon, William Collins, Jan Fuglestvedt, Jianping Huang, Dorothy Koch et al. 2013. "Anthropogenic and Natural Radiative Forcing." In *Climate Change 2013: The Physical Science Basis, Contribution of Working Group I to the Fifth Assessment Report of the Intergovernmental Panel on Climate Change*, 658-740.

[4] Noel, Lance, Joseph F. Brodie, Willett Kempton, Cristina L. Archer, and Cory Budischak. 2017. "Cost minimization of generation, storage, and new loads, comparing costs with and without externalities." *Applied Energy* 189 (December): 110-121.

[5] Erickson, Peter, Sivan Kartha, Michael Lazarus, Kevin Tempest. 2015. "Assessing carbon lock-in." *Environmental Research Letters* 10, no. 8 (August): 1-7.

[6] Unruh, Gregory C. 2000. "Understanding carbon lock-in." *Energy policy* 28, no. 12 (October): 817-830.

[7] Mignone, Bryan K., Sharon Showalter, Frances Wood, Haewon McJeon, Daniel Steinberg. 2017. "Sensitivity of natural gas deployment in the US power sector to future carbon policy expectations." *Energy Policy* 110 (November): 518-524.

[8] Lynch, Peter. 2008. "The ENIAC Forecasts: A Re-Creation." *Bulletin of the American Meteorological Society*. January 1, 2008. https://doi.org/10.1175/BAMS-89-1-45

[9] Edwards, Paul N. 2012. "Entangled histories: Climate science and nuclear weapons research." *Bulletin of the Atomic Scientists*. 68, no. 4 (July): 28-40. http://journals.sagepub.com/doi/abs/10.1177/0096340212451574

[10] Marshall, John, R. Alan Plumb. 2008. *Atmosphere, Ocean, and Climate Dynamics*.

[11] Lions, Jacques Louis, Roger Teman, Shouhong Wang. 1992. "New formulations of the primitive equations of atmosphere and applications." *Nonlinearity* 5, no.2: 237-288.

[12] American Chemical Society. "A Single-Layer Atmosphere Model." *ACS Climate Science Toolkit*. Accessed December 9, 2017.

[13] Manabe, Syukuro, Richard T. Wetherald. "Effects of Doubling the CO_2 Concentration on the Climate of a General Circulation Model." *Journal of the Atmospheric Sciences*. Vol. 32, No. 1. January 1975.

[14] Simpson, Isla. "The equations governing atmospheric flow." *Advanced Atmospheric Dynamics*. 2010. National Center for Atmospheric Research Climate and Global Dynamics Laboratory.

[15] Flato, Gregory, Jochem Marotzke, Babatunde Abiodun, Pascale Braconnot, Sin Chan Chou, William J. Collins, Peter Cox et al. 2013. "Evaluation of Climate Models." In *Climate Change 2013: The Physical Science Basis, Contribution of Working Group I to the Fifth Assessment Report of the Intergovernmental Panel on Climate Change*, 741-866.

[16] Kolstad, Charles, Kevin Urama, John Broome, Annegrete Bruvoll, Micheline Cariño-Olvera, Don Fullerton, Christian Gollier et al. 2014. "Social, economic and ethical concepts and methods." In *Climate Change 2014: Mitigation of Climate Change, Contribution of Working Group III to the Fifth Assessment Report of the Intergovernmental Panel on Climate Change*, 173-248.

[17] Pindyck, Robert S. 2011. "Modeling the Impact of Warming in Climate Change Economics." In *The Economics of Climate Change: Adaptations Past and Present*, edited by Gary D. Libecap and Richard H. Steckel, 47-71. University of Chicago Press. http://www.nber.org/chapters/c11982

[18] Hsiang, Solomon. 2016. "Climate econometrics." *Annual Review of Resource Economics* 8 (2016): 43-75.

[19] Hsiang, Solomon, Robert Kopp, Amir Jina, James Rising, Michael Delgado, Shashank Mohan, D. J. Rasmussen et al. 2017. "Estimating economic damage from climate change in the United States." Science 356, no. 6345 (June): 1362-1369.

[20] Roson, Roberto, and Martina Sartori. 2016. "Estimation of climate change damage functions for 140 regions in the GTAP9 database." *Word Bank Policy Research Working Paper*, no. 7728 (June): 1-42.

[21] Goulder, Lawrence H., and Roberton C. Williams III. 2012. "The choice of discount rate for climate change policy evaluation." *Climate Change Economics* 3, no. 04 (November): 1250024.

[22] Gollier, Christian, and Angela Pachon. 2016. "Computing the Right Price Signal for the Social Cost of Carbon." Kleinman Center for Energy Policy, University of Pennsylvania. April 28, 2016. http://kleinmanenergy.upenn.edu/policy-digests/computing-right-price-signal-social-cost-carbon

[23] Dietz, Simon, Christian Gollier, and Louise Kessler. 2017. "The climate beta." *Centre for Climate Change Economics and Policy Working Paper*, no. 215. *Grantham Research Institute on Climate Change and the Environment Working Paper*, no. 190.

[24] Interagency Working Group on Social Cost of Greenhouse Gases, United States Government. 2016. "Technical Support Document: Technical Update of the Social Cost of Carbon for Regulatory Impact Analysis Under Executive Order 12866." https://www.epa.gov/sites/production/files/2016-12/documents/sc_co2_tsd_august_2016.pdf

[25] Gayer, Ted, W. Kip Viscusi. 2016. "Determining the Proper Scope of Climate Change Policy Benefits in U.S. Regulatory Analyses: Domestic versus Global Approaches." *Review of Environmental Economics and Policy* 10, no. 2 (August): 245-263.

[27] Environmental Protection Agency. 2017. "Repeal of Carbon Pollution Emission Guidelines for Existing Stationary Sources: Electric Utility Generating Units." October 10, 2017.

[28] Revesz, Richard L., Jason A. Schwartz, Peter H. Howard, Kenneth Arrow, Michael A. Livermore, Michael Oppenheimer, Thomas Sterner. 2017. “Letter – The Social Cost of Carbon: A Global Imperative.” *Review of Environmental Economics and Policy* 11, no. 11 (January): 172-173.

[29] Howard, Peter, Jason Schwartz. 2016. “Think Global: International Reciprocity as Justification for a Global Social Cost of Carbon.” *Columbia Journal of Environmental Law* 42 (March): 203-294.

[30] National Academy of Engineering. 2003. “Greatest Engineering Achievements of the 20th Century.” Last updated 2017. http://www.greatachievements.org/

[31] Neidhofer, Gerhard. 2007. "Early three-phase power [History]." *IEEE Power and Energy Magazine* 5, no. 5 (November): 88-100.

[32] Wang, Yongge. 2013. "Smart Grid, Automation, and SCADA systems security." *Security and Privacy in Smart Grids* (2013): 245-268.

[33] Kothari, Dwarkadas Pralhaddas. 2012. "Power system optimization." In *Computational Intelligence and Signal Processing (CISP), 2012 2nd National Conference on*, pp. 18-21. IEEE, 2012.

[34] Boyd, Erin. 2016. “Overview of Power Sector Modeling.” Department of Energy Office of Energy Policy and Systems Analysis. 2016. Accessed October 10, 2017. https://energy.gov/sites/prod/files/2016/02/f29/EPSA_Power_Sector_Modeling_020416.pdf

[35] U.S. Energy Information Administration. 2013. “The Electricity Market Module.” *National Energy Modeling System Model Documentation 2013*. July 2013.

[36] Frew, Bethany A., Mark Z. Jacobson. 2016. “Temporal and spatial tradeoffs in power system modeling with assumptions about storage: An application of the POWER model.” *Energy* 117 (October): 198-213.

[37] Cain, Mary B., Richard P. O’Neill, Anya Castillo. 2012. “History of Optimal Power Flow and Formulations.” *Federal Energy Regulatory Commission*. December 2012. Accessed September 10, 2017. https://www.ferc.gov/industries/electric/indus-act/market-planning/opf-papers/acopf-1-history-formulation-testing.pdf

[38] Krishna, Jayendra, Laxmi Srivastava. “Counterpropagation Neural Network for Solving Power Flow Problem.” *International Journal of Electrical and Computer Engineering* 1, no. 1 (2006): 350-355.

[39] Athavale, Prashant. “Kirchhoff’s Current Law and Kirchhoff’s Voltage Law.” Johns Hopkins Department of Applied Mathematics & Statistics. Accessed October 1, 2017.

[40] Ulaby, Fawwaz T., Michel M. Maharbiz, Cynthia M. Furse. 2016. *Circuits*. Third Edition. National Technology and Science Press.

[41] Momoh, James A. 2009. *Electric Power System Applications of Optimization.* Second Edition. CRC Press.

[42] Abido, M.A. 2002. “Optimal power flow using particle swarm optimization.” *International Journal of Electrical Power & Energy Systems* 24, no. 7 (October): 563-571.

[43] Paucar, Leonardo, Marcos Rider. 2002. “Artificial neural networks for solving the power flow problem in electric power systems.” *Electric Power Systems Research* 62, no. 2 (June): 139-144.

[44] Sun, Andy, and Dzung T. Phan. "Modern Optimization Models and Techniques for Electric Power Systems Operation." *Electric Power System Operations*. Accessed November 15, 2017. http://www2.isye.gatech.edu/~xsun84/publications/OptimizationPowerSystems_final.pdf

[45] Bakirtzis, Anastasios G., Pandel N. Biskas, Christoforos E. Zoumas, and Vasilios Petridis. 2002. "Optimal power flow by enhanced genetic algorithm." *IEEE Transactions on power Systems* 17, no. 2 (2002): 229-236.

[46] Nguyen, T. T. 1997. “Neural network optimal-power-flow.” *International Conference on Advances in Power System Control, Operation and Management*. (1997): 266-271.

[47] Garcia, Alfredo, Lamine Mili, James Momoh. 2010. “Modeling Electricity Markets: A Brief Introduction.” Economic Market Design and Planning. *Institute of Electrical and Electronics Engineers* (2010): 21-44.

[48] Ethier, Robert, Ray Zimmerman, Timothy Mount, William Schulze, Robert Thomas. 1999. “A uniform price auction with locational price adjustments for competitive electricity markets.” *Electric Power and Energy Systems* 21, no. 2 (1999): 103-110.

[49] Lima, Victor O. “The Planning Problem.” *Elements of Economic Analysis II*. The University of Chicago. Accessed October 10, 2017.

[50] Hart, Elaine K., Eric D. Stoutenburg, Mark Z. Jacobson. 2012. “The Potential of Intermittent Renewables to Meet Electric Power Demand: Current Methods and Emerging Analytical Techniques.” *Proceedings of the IEEE* 100, no. 2 (February): 322-334.

[51] Frey, H. Christopher, David E. Burmaster. 1999. “Methods for Characterizing Variability and Uncertainty: Comparison of Bootstrap Simulation and Likelihood-Based Approached.” *Risk Analysis* 19, no. 1 (1999): 109-130.

[52] Cochran, Jaquelin, Lori Bird, Jenny Heeter, Douglas J. Arent. 2012. “Integrating Variable Renewable Energy in Electric Power Markets: Best Practices from International Experience.” National Renewable Energy Laboratory. Accessed July 10, 2017. https://www.nrel.gov/docs/fy12osti/53730.pdf

[53] Orwig, K. D., Ahlstrom, M. L., Banunarayanan, V., Sharp, J., Wilczak, J. M., Freedman, J., ... & Hodge, B. M. 2015. Recent trends in variable generation forecasting and its value to the power system. *IEEE Transactions on Sustainable Energy* 6, no. 3 (2015): 924-933.

[54] Sharma, N., Sharma, P., Irwin, D., & Shenoy, P. 2011. Predicting solar generation from weather forecasts using machine learning. *IEEE International Conference on Smart Grid Communications* (October): 528-533.

[55] Chakraborty, P., Marwah, M., Arlitt, M. F., & Ramakrishnan, N. 2012. Fine-Grained Photovoltaic Output Prediction Using a Bayesian Ensemble. *AAAI* 26 (2012): 274-280.

[56] Blair, Nate, Ella Zhou, Dan Getman, Douglas J. Arent. 2015. "Electricity Capacity Expansion Modeling, Analysis, and Visualization: A Summary of Selected High-Renewable Modeling Experiences." National Renewable Energy Laboratory. October 2015. Accessed October 1, 2017. https://www.nrel.gov/docs/fy16osti/64831.pdf

[57] Jacobson, Mark Z., Mark A. Delucchi, Zack AF Bauer, Savannah C. Goodman, William E. Chapman, Mary A. Cameron, Cedric Bozonnat et al. 2017. "100% clean and renewable wind, water, and sunlight all-sector energy roadmaps for 139 countries of the world." *Joule* 1, no. 1 (2017): 108-121.

[58] Hirth, Lion. 2015. "The Optimal Share of Variable Renewables." *The Energy Journal* 36, no. 1 (2015): 127-162.

[59] Bistline, John E., and Geoffrey J. Blanford. 2016. "More than one arrow in the quiver: Why "100% renewables" misses the mark." *Proceedings of the National Academy of Sciences* (2016): 201603072.

[60] Budischak, Cory, DeAnna Sewell, Heather Thomson, Leon Mach, Dana E. Veron, Willet Kempton. 2013. "Cost-minimized combinations of wind power, solar power and electrochemical storage, powering the grid up to 99.9% of the time." *Journal of Power Sources* 225 (March): 60-74.

[61] Cheng, Luke L. 2014. "Solar, Wind, and Storage: Optimizing for Least Cost Configurations of Renewable Energy Generation in the PJM Grid." Princeton University. June 2014. Accessed July 1, 2017. http://arks.princeton.edu/ark:/88435/dsp012j62s504h

[62] PJM Interconnection. 2017. "PJM's Evolving Resources Mix and System Reliability." March 30, 2017. Accessed June 4, 2017. http://www.pjm.com/~/media/library/reports-notices/special-reports/20170330-pjms-evolving-resource-mix-and-system-reliability.ashx

[63] Bolinger, Mark. 2017. "Using Probability of Exceedance to Compare the Resource Risk of Renewable and Gas-Fired Generation." Lawrence Berkeley National Laboratory. March 23, 2017.

[64] Jenkin, Thomas, Victor Diakov, Easan Drury, Brian Bush, Paul Denholm, James Milford, Doug Arent, Robert Margolis, and Ray Byrne. "The Use of Solar and Wind as a Physical Hedge against Price Variability within a Generation Portfolio." National Renewable Energy Laboratory. August, 2013.

[65] Glasner, Eli, and Benjamin Weiss. "Sensitive dependence on initial conditions." *Nonlinearity* 6, no. 6 (1993): 1067.

[66] Mnyukh, Yuri. 2013. "Hysteresis of Solid-State Reactions: Its Cause and Manifestations." *American Journal of Condensed Matter Physics* 3, no. 5. (2013): 142-150.

[67] Jiles, D.C., D.L. Atherton. 1986. "Theory of ferromagnetic hysteresis." *Journal of Magnetism and Magnetic Materials* 61, no.1-2. (September): 48-60.

[68] Sasaki, Tsuyoshi, Yoshio Ukyo, Petr Novak. 2013. “Memory effect in a lithium-ion battery.” *Nature Materials* 12 (2013): 569-575.

[69] Arthur, W. Brian. 1989. “Competing Technologies, Increasing Returns, and Lock-In by Historical Events.” *The Economic Journal* 99 (March): 116-131. Royal Economic Society.

[70] Liebowitz, Stan J., Stephen E. Margolis. 1995. “Path Dependence, Lock-In, and History.” *Journal of Law, Economics and Organization* 11 (1995): 205-226. SSRN.

[71] Blum, Avrim, MohammadTaghi Hajiaghayi, Katrina Ligett, and Aaron Roth. 2008. "Regret minimization and the price of total anarchy." In *Proceedings of the fortieth annual ACM symposium on Theory of computing* (May): 373-382.

[72] Bell, David E. 1982. "Regret in Decision Making Under Uncertainty." *Operations Research* 30, no. 5 (1982): 961-981.

[73] Loomes, Graham, and Robert Sugden. "Regret Theory: An Alternative Theory of Rational Choice Under Uncertainty." *The Economic Journal* 92, no. 368 (1982): 805-824.

[74] Miranda, Vladimiro, L. M. Proenca. 1998. “Why Risk Analysis Outperforms Probabilistic Choice as the Effective Decision Support Paradigm for Power System Planning.” *IEEE Transactions on Power Systems* 13, no. 2 (May): 643-648.

[75] Blum, Avrim, and Yishay Monsour. 2007. "Learning, regret minimization, and equilibria." *Research Showcase*. Carnegie Mellon University.

[76] Evers, Lanah, Twan Dollevoet, Ana Isabel Barros, and Herman Monsuur. "Robust UAV mission planning." *Annals of Operations Research* 222, no. 1 (2014): 293-315.

[77] Balmann, Alfons, Martin Odening, Hans-Peter Weikard, Wilhelm Branded. 1996. “Path-dependence without increasing returns to scale and network externalities.” *Journal of Economic Behavior & Organization* 29, no. 1 (January): 159-172.

[78] Dixit, Avinash. 1989. “Hysteresis, Import Penetration, and Exchange Rate Pass-Through.” *The Quarterly Journal of Economics* 104, no. 2 (May): 205-228.

[79] Baldwin, Richard. 1989. “Sunk Cost Hysteresis.” *Working Paper Series*. National Bureau of Economic Research. March, 1989. http://www.nber.org/papers/w2911

[80] Stockman, Lorne. 2017. “Gas Pipeline Methodology: Calculating Greenhouse Gas Emissions for Natural Gas Infrastructure.” Oil Change International. Winder 2017. Accessed December 1, 2017.
http://priceofoil.org/content/uploads/2017/02/Gas-Pipeline-Methodology-2017-Web-Final.pdf

[81] Marechal, Kevin. 2007. “The economics of climate change and the change of climate in economics.” *Energy Policy*. Vol. 35, Issue 10. October 2007. p.5181-5194.

[82] Parenteau, Patrick, and Abigail Barnes. 2012. “A Bridge Too Far: Building Off-Ramps on the Shale Gas Superhighway.” *Idaho Law Review* 49 (2012): 325-365.

[83] Ren, Xinrong, Dolly L. Hall, Timothy Vinciguerra, Sarah E. Benish, Phillip R. Stratton, Doyeon Ahn, Jonathan R. Hansford et al. 2017. "Methane emissions from the Marcellus Shale in

southwestern Pennsylvania and northern West Virginia based on airborne measurements." *Journal of Geophysical Research: Atmospheres* 122, no. 8 (2017): 4639-4653.

[84] Zhang, Xiaochun, Nathan P. Myhrvold, Zeke Hausfather, and Ken Caldeira. 2016. "Climate benefits of natural gas as a bridge fuel and potential delay of near-zero energy systems." *Applied Energy* 167 (2016): 317-322.

[85] NREL. "Wind Toolkit Data Downloads." NREL Developer Network. Accessed August 8, 2017. https://developer.nrel.gov/docs/wind/wind-toolkit/

[86] Draxl, C., B. M. Hodge, A. Clifton, and J. McCaa. 2015. "Overview and Meteorological Validation of the Wind Integration National Dataset Toolkit." National Renewable Energy Laboratory. April 2015. Accessed August 8, 2017. https://www.nrel.gov/docs/fy15osti/61740.pdf

[87] NREL. "WIND Toolkit Power Data Site Index." NREL Data Catalog. Accessed September 1, 2017. https://data.nrel.gov/submissions/54

[88] NREL. "Solar Integration National Dataset Toolkit." NREL Grid Modernization. Accessed September 1, 2017. https://www.nrel.gov/grid/sind-toolkit.html

[89] NREL. "Solar Power Data for Integration Studies." NREL Grid Modernization. Accessed September 1, 2017. https://www.nrel.gov/grid/solar-power-data.html

[90] Grana, Paul. 2016. "Solar inverters and clipping: What DC/AC inverter load ratio is ideal?" *Solar Power World*. July 8, 2016. Accessed September 15, 2017. https://www.solarpowerworldonline.com/2016/07/solar-inverters-clipping-dcac-inverter-load-ratio-ideal/

[91] Blue Oak Energy. 2015. "The Ideal Inverter Loading Ratio (ILR) for Commercial and Utility Solar Plants." November 18, 2015. Accessed September 15, 2017. http://www.blueoakenergy.com/blog/inverter-loading-ratio/

[92] Fedkin, Mark. 2017. "Utility Solar Power and Concentration: Efficiency of Inverters." Penn State College of Earth and Mineral Sciences. Accessed September 15, 2017. https://www.e-education.psu.edu/eme812/node/738

[93] Lalonde, Louis. 2011. "Don't Judge a Solar PV System's Efficacy by Inverter Efficiency Alone." *Electronic Design*. October 25, 2011. http://www.electronicdesign.com/energy/don-t-judge-solar-pv-system-s-efficacy-inverter-efficiency-alone

[94] PJM. "Metered Load Data." PJM Markets & Operations. Accessed September 5, 2017. http://www.pjm.com/markets-and-operations/ops-analysis/historical-load-data.aspx

[95] Burke, James V. "Markowitz Mean-Variance Portfolio Theory." *Nonlinear Optimization*. University of Washington. Spring 2014.

[96] McCalley, Jim. 2005. "Loads and Load Duration." *Introduction to Energy Distribution Systems*. Iowa State University Department of Electrical & Computer Engineering. Accessed November 1, 2016.

[97] Energy Information Administration. 2017. “Table 8.2. Cost and performance characteristics of new central station electricity generating technologies.” *Annual Energy Outlook 2017*. Accessed September 1, 2017. https://www.eia.gov/outlooks/aeo/assumptions/pdf/table_8.2.pdf

[98] Energy Information Administration. “Carbon Dioxide Emissions Coefficients.” February 2, 2016. Accessed October 1, 2017. https://www.eia.gov/environment/emissions/co2_vol_mass.php

[99] International Gas Union. “Natural Gas Conversion Guide.” 2012. Accessed October 10, 2017. http://agnatural.pt/documentos/ver/natural-gas-conversion-guide_cb4f0ccd80ccaf88ca5ec336a38600867db5aaf1.pdf

[100] Haratyk, Geoffrey. 2017. “Early Nuclear Retirements in Deregulated U.S. Markets: Causes, Implications and Policy Options.” *Working Paper Series*. MIT Center for Energy and Environmental Policy Research. March 2017.

[101] Monitoring Analytics. 2017. “Generation and Transmission Planning, Table 12-11.” *Quarterly State of the Market Report for PJM*. 2017. Accessed October 1, 2017. http://www.monitoringanalytics.com/reports/PJM_State_of_the_Market/2017/2017q2-som-pjm-sec12.pdf